NASA TECHNICAL MEMORANDUM

NASA TM X-2607

NASA TM X-2607

FLIGHT INVESTIGATION OF AN AIR-COOLED PLUG NOZZLE WITH AN AFTERBURNING TURBOJET

by Nick E. Samanich

Lewis Research Center

Cleveland, Ohio 44135

NATIONAL AERONAUTICS AND SPACE ADMINISTRATION • WASHINGTON, D. C. • SEPTEMBER 1972

1. Report No.	2. Government Accession No.	3. Recipient's Catalog No.
NASA TM X-2607		

4. Title and Subtitle	5. Report Date
FLIGHT INVESTIGATION OF AN AIR-COOLED PLUG NOZZLE WITH AN AFTERBURNING TURBOJET	September 1972
	6. Performing Organization Code

7. Author(s)	8. Performing Organization Report No.
Nick E. Samanich	E-6676
	10. Work Unit No. 764-74
9. Performing Organization Name and Address Lewis Research Center National Aeronautics and Space Administration Cleveland, Ohio 44135	11. Contract or Grant No.
	13. Type of Report and Period Covered Technical Memorandum
12. Sponsoring Agency Name and Address National Aeronautics and Space Administration Washington, D. C. 20546	14. Sponsoring Agency Code

15. Supplementary Notes

16. Abstract

A convectively cooled plug nozzle, using 4 percent of the engine air as the coolant, was tested in 1967 K (3540° R) temperature exhaust gas. No significant differences in cooling characteristics existed between flight and static results. At flight speeds above Mach 1.1, nozzle performance was improved by extending the outer shroud. Increasing engine power improved nozzle efficiency considerably more at Mach 1.2 than at 0.9. The effect of nozzle pressure ratio and secondary weight flow on nozzle performance are also presented.

17. Key Words (Suggested by Author(s))

Propulsion system
Plug nozzle
Heat transfer
Flight test
Transonic

18. Distribution Statement

Unclassified - unlimited

19. Security Classif. (of this report)	20. Security Classif. (of this page)	21. No. of Pages	22. Price*
Unclassified	Unclassified	55	$3.00

* For sale by the National Technical Information Service, Springfield, Virginia 22151

FLIGHT INVESTIGATION OF AN AIR-COOLED PLUG NOZZLE WITH AN AFTERBURNING TURBOJET

by Nick E. Samanich

Lewis Research Center

SUMMARY

A cooled plug nozzle was tested on an afterburning J85-GE-13 turbojet installed under the wing of an F-106B aircraft at Mach numbers from 0.39 to 1.3. The plug nozzle, which utilized a parallel flow convective cooling scheme, was successfully cooled with 4 and 1.8 percent of the engine primary air taken from the compressor discharge when subjected to exhaust gas temperatures as high as 1967 K (3540° R) and 1515 K (2727° R), respectively. No significant differences in cooling characteristics were observed during the flight tests compared with results obtained earlier in a static facility.

The nozzle gross thrust coefficient peaked at Mach 0.945 for all the power settings tested. At this Mach number, the nozzle was in a high pressure field resulting from a terminal shock located just upstream of the nozzle assembly. The pressure rise behind the shock was amplified by the presence of the aircraft wing. The effect of varying the power setting on nozzle performance was significantly more pronounced at the higher Mach numbers. At comparable operating conditions, increasing power from military to maximum afterburning increased the nozzle gross thrust coefficient approximately 6.5 counts at Mach 0.9 and 16.5 counts at Mach 1.2.

At flight speeds above Mach 1.1 and with the engine in maximum afterburning, the nozzle gross thrust coefficient was increased when the outer shroud was extended from a retracted to an intermediate position. The effect of nozzle pressure ratio and secondary weight flow on nozzle performance is also presented.

INTRODUCTION

The plug nozzle has been of general interest for many years for use with advanced propulsion systems. It offers good aerodynamic performance, has a low infrared signature, and can operate efficiently over a range of pressure ratios with minimal

geometry changes (refs. 1 to 9). Because of concern regarding the feasibility associated with various cooling schemes, the use of plug nozzles to date has been limited to systems having low or moderate exhaust gas temperatures. Various plug cooling techniques have been under study for several years (refs. 10 to 15), they range from cooling the plug with engine fuel to using air convectively, as a film, or a combination thereof. The performance penalty associated with these cooling techniques becomes important if any comparisons of nozzle types are to be made. If engine fuel is used, engine cycle efficiency is not affected, and the penalty is only one of system weight, complexity, and reliability. However, if engine bleed air is used, it becomes necessary to know the required quantity to adequately assess the performance penalty. In an attempt to establish plug nozzle cooling requirements, a full-scale air-cooled plug nozzle was designed, built, and tested with a General Electric J85-13 afterburning turbojet (ref. 10). It was demonstrated that a plug nozzle could be convectively cooled with about $3\frac{1}{2}$ percent of the primary engine airflow bled from the compressor discharge with average exhaust gas temperatures as high as 1860 K (3350° R).

In order to establish whether external flow aggravates the nozzle cooling requirements and to measure the installed nozzle performance, the "cooled plug" (ref. 10) was packaged in a flight nacelle and tested on a F-106B aircraft (refs. 16 and 17). The aft mounted under-wing nacelle (fig. 1) had a normal shock inlet and contained a J85-GE-13 turbojet. The 10° half-angle conical plug was tested at three power settings attaining maximum exhaust gas temperatures of 1967 K (3540° R). Several external shroud extensions were tested at maximum afterburning conditions. Test variables also included corrected secondary cooling flow from 1.9 to 9.7 percent of primary flow, exhaust nozzle pressure ratio from 2.22 to 5.8, and flight Mach number from 0.39 to 1.3.

The results include the effect of engine power setting, shroud extension, secondary weight flow, and nozzle pressure ratio on the exhaust nozzle thrust characteristics. Properties of the plug coolant as well as external plug pressures and skin temperatures are also presented.

APPARATUS

Installation

Details of the airplane modifications and the nacelle-engine assembly are given in reference 17. A schematic of the research nacelle and plug nozzle is shown in figure 2. The nacelle was located at the 32 percent semispan with a downward incidence of $4\frac{1}{2}^{\circ}$ (relative to the wing chord) so that the aft portion of the nacelle was tangent to the aft wing lower surface. The nacelle had 0° cant and was positioned to provide approximately

0.64-centimeter (0.25-in.) clearance at the wing trailing edge. Details of the wing modifications, nacelle shape, and wide mounting strut used in these tests are given in reference 18.

The gas generator for the plug nozzle was a J85-GE-13 afterburning turbojet engine consisting of an eight-stage, axial-flow compressor directly coupled to a two-stage turbine, an annular combustor, an afterburner, and a variable area primary exhaust nozzle. The variable area nozzle was removed and replaced with a fixed plug body and tested with three fixed primary throat flaps. The plug nozzle was attached to the afterburner exit using a packing gland slip joint. The plug loads were taken out through three struts. Secondary cooling air was supplied from the inlet and metered at the periphery of the compressor face by a calibrated rotary valve.

Several fuel control and mechanical changes were necessitated or made desirable due to the nonstandard mode of operation - afterburning with fixed primary throat areas. These changes included

(1) Separate main engine and afterburner throttles

(2) An auxiliary regulated pressure supply ("false P_3") located in the aircraft wing, which was used to pressurize the afterburner fuel controller permissive port to allow afterburner fuel flow with part speed engine operation

(3) A cockpit controlled valve, which permitted switching from "false P_3" pressure to engine compressor discharge pressure P_3 at the afterburner fuel controller

(4) An automatic speed control capable of controlling engine speed from 85 to 99.5 percent of rated.

The following changes were incorporated as precautionary safety measures because of the increased risk of an engine overspeed resulting from an afterburner flame out with the fixed exit-area mode of operation.

(1) The engine mechanical overspeed governor was readjusted with the flat occurring between 99.6 and 100.0 percent of rated engine speed. (Standard setting is ~106±1 percent of rated engine speed).

(2) A fast response servo system designed to maintain engine speed by controlling the main engine throttle was incorporated. The set point was 100.3 percent of rated speed.

(3) An automatic engine shutdown system set to activate at 100.5 percent of rated speed was also incorporated.

In addition, critical afterburner liner and plug wall temperatures were wired to cockpit warning lights for pilot monitoring during the flight tests. Details of the preflight checkout are presented in appendix A. The aircraft cockpit duel throttle arrangement for the J-85 and the pilot panel display is shown in figure 3.

Test Hardware

The basic plug (see fig. 4) was a 10° half-angle conic body that was attached to a 63.5-centimeter (25.0-in.) nacelle by three equally spaced hollow support struts. The plug was 40.70 centimeters (16.02 in.) at its maximum diameter and 141.71 centimeters (55.79 in.) long. The distance from the throat to the theoretical plug apex was 112.65 centimeters (44.35 in.). Throat area variation was achieved with three fixed primary flaps that permitted engine operation at military, reheat B^+ and maximum afterburning power. The flaps simulated hinged primary leaves and had boattail angles of 17.28°, 13.40°, and 7.57°. Three outer shroud extensions were tested with the engine in maximum afterburning power. They corresponded to a retracted position ($x/\ell = -0.163$) suitable for low-pressure operation and two extended positions ($x/\ell = 0.163$ and 0.343), which might be suitable for a typical flight acceleration profile. Only the retracted shroud was tested with the military and reheat B^+ primaries.

Cooling Details

The plug and strut cooling flow paths are shown in figure 5. Compressor discharge air was obtained from the four customer bleed ports located in the main frame section of the engine and ducted back through four lines to a torroidal distribution manifold. The cross section of the manifold was formed from 7.62-centimeter (3.0-in.) outside-diameter tubing. The final flattened oval shape had major and minor axes of 9.80 centimeters (3.86 in.) and 3.81 centimeters (1.50 in.), respectively, with rounded ends having a radius of 1.91 centimeters (0.75 in.). The mean diameter of the torus was 55.88 centimeters (22.0 in.), and it fit in the annulus between the afterburner liner casing and the nacelle wall approximately 30.48 centimeters (12.0 in.) upstream of the plug nozzle. Three lines routed the plug and strut cooling air from the distribution manifold directly to the three plug support struts. After entering the struts, the coolant was forced toward the strut leading edge then channeled around the sides to the back and dumped into the plug cavity. The coolant then flowed forward through a Venturi passage where it impinged on the inside of the plug dome. It then entered the plug cooling channels, which were made of nickel fins brazed to the 0.157-centimeter (0.062-in.) Inconel 625 outer wall. The fins were 0.794 centimeter (0.313 in.) long, and the circumferential spacing was varied to yield approximately uniform plug wall temperatures at the maximum heat load condition. The coolant passed longitudinally aft and was discharged out of an annulus located at an axial station corresponding to 60 percent of a full length plug. The remaining plug tip was film cooled by the discharged gases. The flow area of the plug exit annular coolant passage during hot operation was calculated to be 28.0 square centimeters ($4.34\ \text{in.}^2$).

The primary flap was film cooled with residual cooling air from the afterburner liner at all power settings; however, this was supplemented when operating in maximum afterburn with film from two additional cooling slots. The two slots, fed by six lines from the distribution manifold, were located immediately upstream and downstream of the plug support struts. In addition, secondary air and (with the retracted shroud) external flow was somewhat effective in convectively cooling the outer side of the primary flap.

All cooling-air lines feeding the plug assembly had provisions for the installation of orifices immediately downstream of the distribution manifold. For the tests with military engine power, all nine lines were fitted with solid blanks preventing any cooling-air flow. For reheat B^+ engine operation, the six lines feeding the film cooling manifolds were blanked and 1.21 centimeter (0.475 in.) diameter orifices were used in the three lines supplying strut and plug cooling air. The three lines to the struts were left open (no orifices) and 0.823-centimeter (0.324-in.) diameter orifices were used in the other six lines for tests in maximum afterburning. The orifices were sized during static testing in an altitude facility to minimize cooling flow rates at the various power settings.

Instrumentation

Although the plug nozzle had extensive instrumentation built into the hardware (ref. 10), only a selected number of thermocouples were used during the flight tests. The coordinate system used to locate the instrumentation is shown in figure 6 and a complete tabulation of the pressure and temperature measurement locations on the plug is made in table I. In addition to a skin temperature measurement, the three flaps tested had 12 area weighted pressure taps located as shown in figure 7. Also shown in the secondary flow instrumentation, four total-pressure and temperature probes attached to the outer shrouds with the survey plane near the secondary flow exit. Compressor bleed air was used for plug cooling when afterburning. During static check out of the plug assembly total and static pressures were used in the four calibrated compressor discharge lines to measure total coolant flow. Similar instrumentation was used in the three lines supplying coolant to the struts and plug. During the flight testing, the quantity of plug coolant flow was calculated in a similar manner but primary flap film coolant was estimated as being the same constant percentage of plug coolant as that measured in the static testing. Compressor discharge pressure P_3 was also monitored at one of the customer air attachment ports.

The inlet, secondary air valve, and compressor face instrumentation are shown in figure 8. Additional engine instrumentation included fuel flowmeters, an engine speed sensor, and pressure and temperature surveys at the turbine discharge (ref. 16).

A flight calibrated test boom located on the aircraft nose was used to determine free-stream static and total pressures and aircraft angle-of-attack and sideslip angle.

Photographs of some of the plug nozzle components are shown in figures 9 to 14. The five assemblies flight tested are shown installed on the F-106B aircraft in figure 15.

PROCEDURE

All flights were made out of Selfridge Air Force Base in Mt. Clemans, Michigan, with a test corridor over Lake Huron used during data acquisition. A total of eight flights were made during this test series. A prescribed flight trajectory was followed, which resulted in a repeatable angle-of-attack and elevon-deflection schedule (see fig. 16). For the data taken at a nominal 0.4 Mach number, the aircraft was at a pressure altitude h of 228.6 meters (750 ft), an angle-of-attack α of 6.5°, and had a nominal elevon deflection δ of 3° on the wing above the plug nozzle.

For the afterburning configurations, a predetermined operating procedure was followed (see appendix A). The procedure established was based on being operationally safe and one that minimized fuel consumption prior to data acquisition.

The "false P_3" pressure used to activate one of the afterburner fuel permissives was set prior to flight to a value that would provide fuel flow conditions adequate for an afterburner light and would also match conditions during the transition to engine P_3. The predetermined gage values were 3.0338×10^5 and 3.1717×10^5 newtons per square meter (44 and 46 psi) for the reheat B^+ and maximum afterburner primaries, respectively. The J-85 main burner was lit shortly after takeoff. Afterburner ignition was made at an engine speed of 75 percent N_R, Mach number M_0 of 0.5, and an altitude of 4572 meters (15 000 ft) for the reheat B^+ primary and 80 percent N_R, 0.4 Mach, and 3048-meter (10 000-ft) altitude for the maximum afterburning primary. Attempts to light-off at the predetermined 80 percent N_R were unsuccessful with the reheat B^+ primary. It was speculated that the colder in-flight compressor face air temperature $T_2 = 258$ K (465° R), compared with that during the static ignition limit tests (appendix A), was the cause. After successful light-off, engine speed was advanced using both throttles and keeping turbine discharge temperature in the "safe" T_5 corridor. Upon reaching 95 percent of rated speed, the transition to engine P_3 and engine speed control was made. The aircraft was then accelerated, and the altitude changed corresponding to conditions desired for data acquisition. Just before data acquisition, the engine speed was increased to rated and the afterburner throttle advanced until rated T_5 temperature was reached. These conditions correspond to rated afterburner power at the nozzle throat area being tested. With some of the configurations tested, data were taken at various T_5 temperatures and secondary cooling flows.

DATA REDUCTION

Engine airflow was determined using prior engine calibration data (ref. 19) along with in-flight measurements of engine speed, pressure, and temperature at the compressor face. Total temperature T_8, total pressure P_8, and effective area A_{E8} were obtained by using the values of engine airflow, engine and afterburner fuel flows, the total pressure and temperature at the turbine discharge, along with afterburner temperature rise and pressure drop calibration results. Calibrations of the secondary-flow-valve pressure drop and position were used to determine secondary airflow. Compressor bleed air, used for plug cooling in the afterburning configurations, was determined from line orifice pressure drops and previous flow calibrations. The quantity of bleed air used for supplemental film cooling of the primary flaps when in maximum afterburn was included in the primary weight flow w_8.

Prior in-flight thrust system calibrations were made with reference cylindrical ejectors. The ejector thrust characteristics in conjunction with the load-cell readings were used to determine a nacelle tare force. The tare force, consisting of the inlet momentum and all external forces on the nacelle forward of the nozzle attachment flange (nacelle station 457.2 cm (180 in.)), was shown to be a function of flight speed and inlet spillage. Knowing these two parameters during the research flights enabled the tare to be determined. The load-cell measurement was used in combination with the tare force to determine nozzle gross thrust minus drag. Details of the calibrations and of the thrust-measuring system for the F-106 are presented in reference 16.

The basic nozzle performance parameter selected was a ratio of measured gross thrust minus drag ratioed to the ideal thrust of the primary flow. The ideal thrust of the primary was calculated from the known mass-flow rate expanded isentropically from its total pressure to ambient pressure p_0. Pressures were integrated over the surfaces of the primary flaps and the calculated axial forces are presented in terms of percent of ideal primary thrust. The axial thrust of the primary, secondary, and plug coolant streams in their respective exit planes was also calculated. Total pressures, temperatures, and weight flows were used with known exit areas to obtain the thrust contributions. The primary and plug coolant forces were adjusted for an assumed 10° flow angularity in their exit planes. Individual pressure distributions along the plug body are also presented.

RESULTS AND DISCUSSION

Performance Characteristics

Three primary throat areas were tested. When operating at rated turbine discharge temperature T_5 the three exit areas corresponded to nominal J85 power settings of military, reheat B^+, and maximum afterburning. The effect on the nozzle gross thrust coefficient $(F - D)/F_{ip}$ is shown in figure 17. The data at military and reheat B^+ power settings were taken with approximately 3.2 percent corrected secondary airflow $\omega\sqrt{\tau}$, while the data at maximum afterburning was taken with approximately 6.5 percent. The shaded area in figure 17, below the afterburning configuration data, represents the momentum of the plug coolant calculated using properties at its discharge plane (Sta 608.2 cm (239.45 in.)). At all three power settings, the peak nozzle gross thrust coefficient occurred at Mach 0.945 followed by a sharp drop at Mach 0.98. At Mach 0.945, a terminal shock was located just upstream of the nozzle assembly. As described in reference 20, the combination of the flow field of the wing and the flow field around the nacelle, which was reflected by the lower surface of the wing, amplified the recompression of the flow through the shock and over the nozzle assembly. These higher pressures reduced the nozzle drag and increased the nozzle performance. A sharp drop in pressure and performance accompanies the terminal shock movement off the nozzle assembly, which occurred at Mach 0.98. An attempt was made to compare the nozzle thrust coefficient at comparable operating conditions in terms of Mach number, nozzle pressure ratio, and plug coolant flows. The performance was adjusted to correspond to that expected with 6.5 percent corrected secondary weight flow $\omega\sqrt{\tau}$, no plug coolant flow thrust, and a nozzle pressure ratio P_8/p_0 of 3.35 and 4.50 at Mach 0.9 and 1.20, respectively. The adjustment in performance was based on a calculated exit momentum of the plug coolant and characteristic variations in performance with secondary coolant flow and nozzle pressure ratio measured in these tests and data reported in reference 9. The data and incremental corrections are tabulated in table II and the final adjusted performance shown as a function of nacelle to primary throat area ratio in figure 18. The data indicate a linear increase in thrust coefficient with increasing throat area. The gross thrust coefficient increased 6.5 and 16.5 counts at Mach 0.90 and 1.2, respectively when the area ratio (A_n/A_{E8}) was decreased from 4.34 to 2.87 (military to maximum afterburner power).

Three external shroud extensions were tested with the engine in maximum afterburning: A fully retracted position suitable for low pressure ratio operation (x/ℓ = -0.163) and two extended positions (x/ℓ = 0.163 and 0.343). The most extended shroud corresponds to one that would be required for optimum performance when operating at typical supersonic cruise pressure ratios. As can be seen in figure 19, there was a slight improvement in performance at flight speeds above Mach 1.1 when the outer shroud was extended from a retracted (x/ℓ = -0.163) to an intermediate position (x/ℓ = 0.163). The

data from cold flow tests on a similar isolated configuration (ref. 5) indicated that shroud translation was not beneficial until a Mach number of approximately 1.50 had been reached, when operating at the same nozzle pressure ratios as in the present investigation.

The effect of secondary weight flow variations on nozzle thrust coefficient is shown in figure 20. The data are presented for the military and reheat B^+ power settings at nominal Mach numbers of 0.9 and 1.2. In general, increasing secondary weight flow 1 percent of the primary flow resulted in a corresponding percent increase in thrust coefficient.

The effect of exhaust nozzle pressure ratio on the nozzle thrust coefficient at Mach 0.9 is shown in figure 21. The limited data obtained at the military and reheat B^+ throat settings indicates similar characteristic trends. The upper values of pressure ratio were limited by attaining rated turbine outlet temperature T_5 at 100 percent rated mechanical speed for the J85 engine. At Mach 0.9 and a reheat B^+ power setting increasing exhaust nozzle pressure ratio from 3.25 to 3.75 increased the nozzle gross thrust coefficient about 3.5 counts.

The engine and coolant flow conditions for all the rated engine points used in the performance evaluation are presented in figure 22 for the military, reheat B^+, and maximum afterburning power. Except for a few incorrect secondary valve settings, the variation in secondary cooling flow over the Mach number range for the military and reheat B^+ power settings is a result of estimating the pumping characteristics prior to the flight tests. The secondary valve was set at full open for the tests with the maximum afterburning primary. The variation in exhaust gas temperature T_8 with all the power settings was primarily due to the inability to set exact engine conditions with the dual throttle control system and the normal variation due to changes in compressor efficiency with Reynold's number.

The integrated pressure measurements on the primary flaps along with calculated primary, secondary, and plug coolant exit momenta are presented over the Mach number range in figure 23(a) and (b) for the military and reheat B^+ power settings, respectively, and in figures 23(c) to (e) for the maximum afterburning configurations. For all configurations with the retracted outer shroud (figs. 23(a) to (c)), the primary flap drag is minimal at Mach 0.945, when the terminal shock is located just ahead of the nozzle assembly and then increases to its peak value at Mach 0.98 when the terminal shock passes off the assembly. With the extended outer shrouds, the primary flap is shielded from external flow effects, and the location of the terminal shock no longer influences the flap drag values. As indicated previously, increases in adjusted nozzle thrust coefficient of 6.5 and 16.5 counts were measured at Mach 0.9 and 1.2, respectively, when increasing the power setting from military to maximum afterburning (see fig. 18). From the component force data (fig. 23) and the data showing the effect of secondary weight flow

(fig. 20), it can be seen that approximately one quarter of the performance increase was due to a reduction in primary flap drag and another one quarter resulted from higher secondary flow momentum. The remaining increase should, therefore, be due to pressure forces on the plug body. Although the measured plug pressures showed an increase, no attempt was made to resolve them into a component force.

Pumping characteristics at Mach 0.9 and 1.2 for the military and reheat B^+ configurations are presented in figure 24. Secondary to primary pressure ratio is shown as a function of corrected secondary weight flow in figures 24(a) and (b). Figure 24(c) shows the effect of nozzle pressure ratio on secondary to primary pressure ratio at Mach 0.9 and at a nominal corrected secondary weight flow ratio $\omega\sqrt{\tau}$ of 0.033. In making any direct comparisons of secondary pressure ratios required to pump comparable corrected secondary weight flows with the different configurations, the reader is reminded that the nozzle pressure ratios P_8/p_0 were not identical and do affect the absolute magnitudes. With the retracted shroud configurations, the secondary pumping is achieved primarily by the external stream rather than the primary jet. However, varying the configuration from the military to maximum afterburning did influence the pumping pressure requirements (fig. 24(d)). It is believed that this effect came about by a change in back pressure at the secondary exit as evidenced by pressure instrumentation on the external side of the primary flap. Primary flap pressures increased when power was increased from military to maximum afterburning probably due to a combination of lowering the primary flap boattail angle β and increasing the exhaust plume diameter because of the larger exit diameter and higher exhaust gas temperatures. An attempt was made to compare the pumping characteristics at the three (retracted shroud) power settings tested at Mach 0.9 at a corrected secondary weight flow $\omega\sqrt{\tau}$ of 0.063. The maximum afterburning thrust coefficient data (fig. 22(c)) and the reheat B^+ data (fig. 24(b)) were adjusted to correspond to a nozzle pressure ratio P_8/p_0 of 3.5. The sensitivity of the reheat B^+ configuration to nozzle pressure ratio (fig. 24(c)) was assumed for both reheat settings. The results indicate an increasing secondary pressure ratio requirement (P_S/P_8 = 0.30, 0.324, and 0.35) as power is increased from military to reheat B^+, to maximum afterburning, respectively, to maintain 0.063 corrected secondary flow at a nozzle pressure ratio of 3.5 and a flight Mach number of 0.9.

Cooling Characteristics

The plug wall and coolant temperature variations, which were obtained statically (ref. 10) and in flight, are compared in figure 25 for the maximum afterburning configuration. An attempt was made to compare data points taken at comparable operating conditions. The quantity of plug coolant was slightly different in maximum afterburning

(about 4 percent in the flight tests compared to $3\frac{1}{2}$ percent of the total weight flow during the static tests). As can be seen, no significant differences appear to exist. The somewhat higher wall temperatures obtained in flight do fall within the data scatter from the ground test and do not indicate any significant temperature changes.

Plug wall temperatures at the throat are presented as a function of exhaust gas temperature and compared with data obtained statically in figure 26. The data indicate an approximately linear increase in wall temperature with increasing exhaust gas temperature with less coolant margin existing with the reheat B^+ power setting. A comparison of the wall temperature variation at the throat (on the primary flap and plug wall) with exhaust gas temperature T_8 at Mach 0.9 is shown in figure 27. At a reheat B^+ power setting, the primary flap temperature increased at a faster rate than the plug wall and was approximately 78 K (140° R) hotter at rated conditions.

Secondary weight flow did not appear to have a measurable effect on the primary flap skin temperature in the reheat B^+ power setting (fig. 28). The data shown are at Mach 0.9 and over a range of corrected secondary weight flows from 0.019 to 0.069.

The plug coolant flow path and measuring stations are shown schematically in figure 29. Coolant pressure and temperature variations along with corresponding metal temperatures are shown at discrete Mach numbers for the afterburning configurations in figure 30. The data are presented for the reheat B^+ and the maximum afterburn primary with retracted, intermediate, and extended shroud in figures 30(a) to (d), respectively. The hottest skin temperatures were measured during the low speed flights ($M_0 \approx 0.4$) and occurred at a station approximately midway between the throat and coolant discharge plane. At Mach numbers greater than 1.0, the hottest metal temperatures occurred near the throat plane. Corresponding pressure distributions along the external plug surface are presented in figure 31 (a) to (d). In addition, the plug pressure variation in military power is presented in figure 31(e). With all the configurations tested, a sharp over expansion occurred immediately aft of the throat followed by a recompression and subsequent pressure oscillations diminishing in intensity. Local pressures immediately downstream of the throat approaching 25 percent of ambient pressure p_0 were recorded at Mach numbers near 1.0.

SUMMARY OF RESULTS

An air-cooled plug nozzle was tested installed under the wing of an F-106B aircraft at Mach numbers from 0.39 to 1.3. Power setting was varied from military to maximum afterburning, and the cooling characteristics compared with data previously obtained in an altitude cell. The effect of power setting, shroud extension, secondary cooling flow and nozzle pressure ratio on the exhaust nozzle thrust characteristics are presented. The following results were obtained:

1. No significant differences in cooling characteristics were observed during the flight tests compared with previous static results.

2. The plug nozzle was adequately cooled using approximately 1.8 and 4.0 percent compressor bleed air with exhaust gas temperatures of 1515 and 1967 K (2727° and 3540° R), respectively.

3. At comparable operating conditions, increasing power setting from military to maximum afterburning increased the nozzle thrust coefficient approximately 6.5 counts at Mach 0.9 and 16.5 counts at Mach 1.2.

4. At Mach numbers above 1.1 and at maximum afterburn power, a slight performance advantage was indicated by extending the outer shroud from a retracted to an intermediate position.

5. A 1-percent increase in corrected secondary weight flow increased nozzle gross thrust coefficient about 1 percent.

6. At Mach 0.9 and a reheat B^{+} power setting increasing exhaust nozzle pressure ratio from 3.25 to 3.75 increased the nozzle gross coefficient approximately $3\frac{1}{2}$ counts.

Lewis Research Center,
National Aeronautics and Space Administration,
Cleveland, Ohio, March 20, 1972,
764-74.

APPENDIX A

PREFLIGHT CHECK-OUT

All of the engine control changes and other modifications were made on a calibrated flight engine (SN244-028) (ref. 19), which was installed in a mock flight nacelle and checked out operationally in an altitude cell. The test program included

(a) Defining the starting envelope and starting sequence for all nozzle exit areas to be flight tested

(b) Sizing appropriate orifices for proper plug coolant flow distribution for the afterburning configurations

(c) Evaluating the adequacy and reliability of the new engine control system

(d) Defining safe operational limits of all critical parameters

(e) Test pilot familiarization and operational experience with the new throttle system.

Interest in the afterburner light-off envelope stemmed from the desire to minimize fuel consumption prior to data acquisition and to obtain safe, smooth, and repeatable lights. The afterburner ignition data obtained are shown in figure 32. All the data presented were obtained with the engine speed at about 80 percent of rated and with an air temperature of about 294 K (530° R) at the compressor inlet. From the data, it was concluded that light-off at 80 percent rated engine speed, Mach 0.4, 3048-meter (10 000-ft) altitude and Mach 0.5, 4572-meter (15 000-ft) altitude with the maximum afterburn and reheat B^+ primaries, respectively, would be satisfactory for the flight tests.

The plug body was designed to withstand maximum skin temperatures of 1222 K (2200° R). The orifice sizing for coolant flow distribution was chosen to allow for some temperature margin for the flight tests. The following orifice sizing was arrived at:

Engine power	Orifice diameter	
	To plug (three lines)	To primary flap (six lines)
Maximum afterburn	Open line (no orifice plate)	0.823 cm (0.324 in.) diam
Reheat B^+	1.21 cm (0.475 in.) diam	Closed line (blank orifice plate)
Military	Closed line (blank orifice plate)	Closed line (blank orifice plate)

The control system checkout was predominantly addressed to defining the dynamic characteristics of the system and its response to an afterburner flame-out. Attempts to simulate a flame-out were made by dropping out the afterburner fuel flow permissive signal which initiated the closing of a fast acting fuel valve. The resulting transient with all control equipment functioning is shown in figure 33. The response of the engine to a ±34 kilonewtons per square meter (±5 psi) pressure differential existing during a transition from "false P_3" to engine P_3 was also examined. No adverse effects were noted.

With the dual throttle control system, it was possible to overheat the nozzle assembly or increase turbine inlet temperature beyond acceptable limits during the transition to rated conditions. In order to minimize the possibility of this happening, a safe operating corridor was empirically established using visual monitoring of the flame intensity in the afterburner with the use of an aft mounted periscope, and the lean blowout limits of the afterburner. This corridor was defined in terms of engine speed and turbine discharge temperature T_5 and is presented

Rated speed, N_R, percent	Turbine discharge temperature T_5	
	K±25	^{o}R±45
80	673	1211
85	698	1256
90	728	1310
95	783	1409
98	813	1463
100	838	1508

In addition, critically located thermocouples were selected for in-flight cockpit monitoring.

After completion of the static checkout, the entire engine assembly was installed in a flight nacelle and mounted to the aircraft. Several ground run-ups in partial afterburning power were made on the aircraft before initiation of the flight program.

APPENDIX B

SYMBOLS

A	area, cm^2 ($in.^2$)
A_{E8}	nozzle effective throat area (hot), cm^2 ($in.^2$)
D	drag, N (lbf)
d	diameter, cm (in.)
F	nozzle gross thrust, N (lbf)
$(F-D)/F_{i,p}$	nozzle gross thrust coefficient
f	component force, N (lbf)
H	perpendicular distance from plug surface, cm (in.)
h	altitude, m (ft)
L	total distance along plug surface from plug front end to coolant exit plane, cm (in.)
l	plug length measured from theoretical throat with military flap to theoretical plug apex, 112.65 cm (44.35 in.)
M	Mach number
N_R	rated engine rotor speed
P	total pressure, N/m^2 abs (psia)
p	static pressure, N/m^2 abs (psia)
T	total temperature, K (^oR)
w	weight flow, kg/sec (lbm/sec)
x	theoretical throat station on plug surface with military primary, station 537.69 cm (211.69 in.)
y	distance along plug surface from plug front end
α	angle of attack, deg
β	primary flap boattail angle, deg
δ	elevon deflection, deg
η	maximum distance from plug surface to primary nozzle
θ	angle, deg

Λ total distance around strut surface

ξ distance along strut surface from reference station

τ secondary flow to primary flow total temperature ratio

ω ratio of secondary to primary weight flow

ω_c ratio of total compressor bleed (plug coolant plus primary film) to primary weight flow

ω_p ratio of plug coolant to primary weight flow

$\omega\sqrt{\tau}$ corrected secondary weight flow ratio

Subscripts:

c coolant

i ideal

n nacelle reference dimension, 63.5 cm (25.0 in.)

p primary gas at throat (station 8)

R rated conditions

S secondary exit, sta 516.26 cm (203.25 in.)

W wall

0 free stream

2 compressor inlet station

3 compressor discharge station

8 primary nozzle throat station

REFERENCES

1. Schmeer, James W.; Kirkham, Frank S.; and Salters, Leland B., Jr.: Performance Characteristics of a 10^{o} Conical Plug Nozzle at Mach Numbers Up to 1.29. NASA TM X-913, 1964.

2. Herd, J. R.; Golesworthy, G. T.; and Herbert, M. V.: The Performance of a Centrebody Propelling Nozzle with a Parallel Shroud in External Flow, Part I. Rep. ARC-CP-841, Aeronautical Research Council, Gt. Britain, 1966.

3. Herbert, M. V.; Golesworthy, G. T.; and Herd, R. J.: The Performance of a Centrebody Propelling Nozzle with a Parallel Shroud in External Flow, Part II. Rep. ARC-CP-894, Aeronautical Research Council, 1966.

4. Bresnahan, Donald L.; and Johns, Albert L.: Cold Flow Investigation of a Low Angle Turbojet Plug Nozzle with Fixed Throat and Translating Shroud at Mach Numbers From 0 to 2.0. NASA TM X-1619, 1968.

5. Bresnahan, Donald L.: Experimental Investigation of a 10^{o} Conical Turbojet Plug Nozzle with Iris Primary and Translating Shroud at Mach Numbers From 0 to 2.0. NASA TM X-1709, 1968.

6. Bresnahan, Donald L.: Experimental Investigation of a 10^{o} Conical Turbojet Plug Nozzle with Translating Primary and Secondary Shrouds at Mach Numbers From 0 to 2.0. NASA TM X-1777, 1969.

7. Harrington, Douglas E.: Performance of a 10^{o} Conical Plug Nozzle with Various Primary Flap and Nacelle Configurations at Mach Numbers From 0 to 1.97. NASA TM X-2086, 1970.

8. Huntley, Sidney C.; and Samanich, Nick E.: Performance of a 10^{o} Conical Plug Nozzle Using a Turbojet Gas Generator. NASA TM X-52570, 1969.

9. Samanich, Nick E.; and Chanberlin, Roger: Flight Investigation of Installation Effects on a Plug Nozzle Installed on an Underwing Nacelle. NASA TM X-2295, 1971.

10. Clark, John S.; Graber, Edwin J.; and Straight, David M.: Experimental Heat Transfer and Flow Results From an Air-Cooled Plug Nozzle System. NASA TM X-52897, 1970.

11. Chenoweth, Francis C.; and Lieberman, Arthur: Experimental Investigation of the Heat Transfer Characteristics of a Film-Cooled Plug Nozzle with Translating Shroud. NASA TN D-6160, 1971.

12. Behiem, Milton A.; Anderson, Bernhard H.; Clark, John S.; Corson, Blake W., Jr.; Stitt, Leonard E.; and Wilcox, Fred A.: Supersonic Exhaust Nozzles. Aircraft Propulsion. NASA SP-259, 1971, pp. 233-282.

13. Stepka, Francis S.; and Chambellan, Rene E.: Feasibility Study of Jet-Fuel-Cooled Plug Nozzle for Afterburning Turbojet. NASA TM X-2304, 1971.

14. Jeracki, Robert J.; and Chenoweth, Francis C.: Coolant Flow Effects on the Performance of a Conical Plug Nozzle at Mach Numbers From 0 to 2.0. NASA TM X-2076, 1970.

15. Clark, John S.; and Lieberman, Arthur: Thermal Design Study of an Air-Cooled Plug-Nozzle System for a Supersonic-Cruise Aircraft. NASA TM X-2475, 1971.

16. Groth, Harold W.; Samanich, Nick E.; and Blumenthal, Philip Z.: Inflight Thrust Measuring System for Underwing Nacelles Installed on a Modified F-106 Aircraft. NASA TM X-2356, 1971.

17. Crabs, Clifford C.; Mikkelson, Daniel C.; and Boyer, Earle O.: An Inflight Investigation of Airframe Effects on Propulsion System Performance at Transonic Speeds. Presented at the 13th Annual Symposium of the Society of Experimental Test Pilots, Los Angeles, Calif., Sept. 25-27, 1969.

18. Mikkelson, Daniel C.; and Head, Verlon L.: Flight Investigation of Airframe Installation Effects on a Variable Flap Ejector Nozzle of an Underwing Engine Nacelle at Mach Numbers From 0.5 to 1.3. NASA TM X-2010, 1970.

19. Antl, Robert J.; and Burley, Richard R.: Steady-State Airflow and Afterburning Performance Characteristics of Four J85-GE-13 Turbojet Engines. NASA TM X-1742, 1969.

20. Wilcox, Fred A.; Samanich, Nick E.; and Blaha, Bernard J.: Flight and Wind Tunnel Investigation of Installation Effects on Supersonic Cruise Exhaust Nozzles at Transonic Speeds. Paper 69-427, AIAA, June 1969.

TABLE I. - PLUG INSTRUMENTATION

[See fig. 6.]

Instrument number	Dimensionless distance along plug surface, y/L	Angle, θ, deg	Instrument number	Dimensionless distance along plug surface, y/L	Angle, θ, deg	Dimensionless perpendicular distance from plug surface, H/η
Plug static pressures (hot gas side)			Plug wall temperatures			
PHPL-1	0	0	TWPL-2	0.0341	10	------
PHPL-2	.1041	357.5	TWPL-3	.0536	5	------
PHPL-3	.2939	0	TWPL-28	.6545	60	------
PHPL-4	.3627	0	TWPL-31	.9909	63.5	------
PHPL-5	.3741	14	TWPL-33	.2995	120.0	------
PHPL-6	.3950	30	TWPL-36	.2995	240.0	------
PHPL-7	.4273	45	TWPL-41	.3684	105.0	------
PHPL-8	.4659	60	TWPL-43	.3684	150.0	------
PHPL-9	.5218	75	TXPL-10	[i]1.303	60.0	------
PHPL-10	.6545	90	Plug coolant temperatures			
PHPL-11	.7491	105				
PHPL-12	.8705	120	TCPL-1	(d)	15.0	------
PHPL-13	.9909	131	TCPL-11	(d)	75.0	------
PHPL-14	.1041	315	TCPL-21	0.3627	18.5	------
PHPL-15	.1352	300	TCPL-22	.3627	48.5	------
PHPL-16	.2405	300	TCPL-31	.9909	20.0	------
PHPL-17	.2939	270	TCPL-32	.9909	50.0	------
PHPL-18	.3627	255	TCPS-9	(f)	120	------
PHPL-19	.3741	239	TCPS-10	(f)	240	------
PHPL-20	.3950	225	Primary flap metal temperature			
PHPL-21	.4273	210				
PHPL-22	.4659	195	TWPS-13	(j)	120.0	------
PHPL-23	.5218	180	Primary flap film temperatures			
PHPL-24	[a]1.092	0				
PHPL-25	[b]1.183	0	TCPS-3	(g)	0	------
PHPL-26	[c]1.341	---	TCPS-5	(h)	0	------
PHPL-27	.2386	358.3	Strut wall temperatures ξ/Λ			
Coolant static pressures						
PCPL-1	0.0511	15	TWST-1	0	0	0.1376
PCPL-8	.9909	10	TWST-10	1.00	↓	.4576
PCPL-16	.9909	70	TWST-13	.4636		.7376
PCPL-17	(d)	45	TWST-15	1.00		.7376
PCPL-18	(e)	180				
PCPL-19	(e)	5				
PCPL-21	.3627	56.5				
PCPS-1	(f)	0				
PCPS-2	(f)	120				
PCPS-3	(f)	240				
PCPS-4	(g)	58				
PCPS-8	(h)	58				
Coolant total pressures						
HCPL-1	0.9909	5				
HCPL-2	↓	22.5				
HCPL-4		65				
HCPL-9		187.5				
HCPL-10		232.5				
HCPL-11		277.5				
HCPL-12		322.5				

[a]Film cooled extension, 10.16 cm (4.0 in.) downstream of film exit.
[b]Film cooled extension, 20.32 cm (8.0 in.) downstream of film exit.
[c]Plug apex.
[d]Impingement pipe; y/L = 0.0705; r = 2.54 cm (1.0 in.).
[e]Plug cavity at strut exit.
[f]Strut inlet.
[g]Forward film manifold.
[h]Aft film manifold.
[i]Film cooled extension, 4.24 cm (1.67 in.) from apex.
[j]Distance from trailing edge, 0.51 cm (0.20 in.).

TABLE II. - INCREMENTAL ADJUSTMENT TO NOZZLE GROSS THRUST COEFFICIENT

MADE TO COMPARE DATA AT MACH 0.9 AND 1.20 (SEE FIG. 18)

[Retracted shroud (x/l = -0.163).]

Power setting	Nacelle to primary throat area ratio, A_n/A_{E8}	Mach number, M_0	Nozzle pressure ratio, P_8/p_0	Corrected secondary weight flow ratio, $\omega\sqrt{\tau}$	Coolant to primary flow ratio		Measured nozzle gross thrust thrust coefficient, $(F-D)/F_{ip}$	Increment due to -			Final nozzle gross thrust coefficient, $(F-D)/F_{ip}$
					Plug coolant, ω_p	Total coolant, ω_c		Plug coolant momentum	$\omega\sqrt{\tau}$ = 0.065	P_8/p_0 = 3.35 at M_0 = 0.90 4.50 at M_0 = 1.20	
Maximum afterburning	2.87	0.9	3.35	0.063	0.040	0.058	1.025	-0.032	+0.002	------	0.995
		1.2	4.5	.069	.041	.058	.980	-.030	-.005	------	.945
Reheat B^+	3.53	0.9	3.75	0.032	0.018	0.018	0.960	-0.011	+0.04	-0.03	0.959
		1.2	5.25	.031	.018	.018	.882	-.012	+.04	-.035	.875
Military	4.34	0.9	3.55	0.032	0	0	0.926	------	+0.030	-0.025	0.931
		1.2	4.64	.029	0	0	.785	------	+.030	-.010	.805

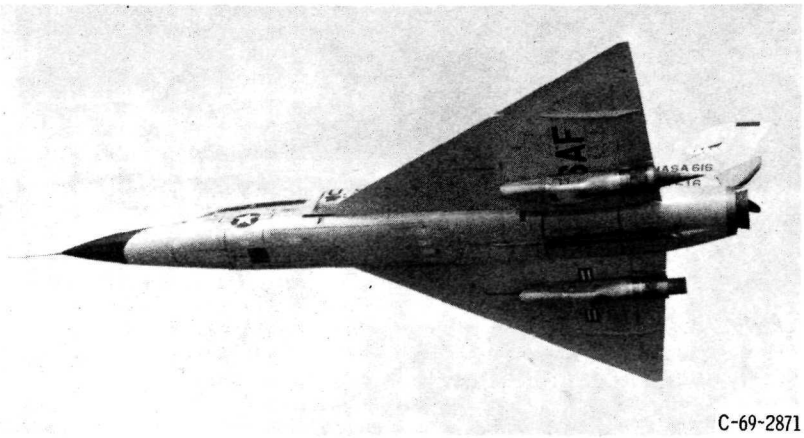

Figure 1. - Modified F-106B aircraft.

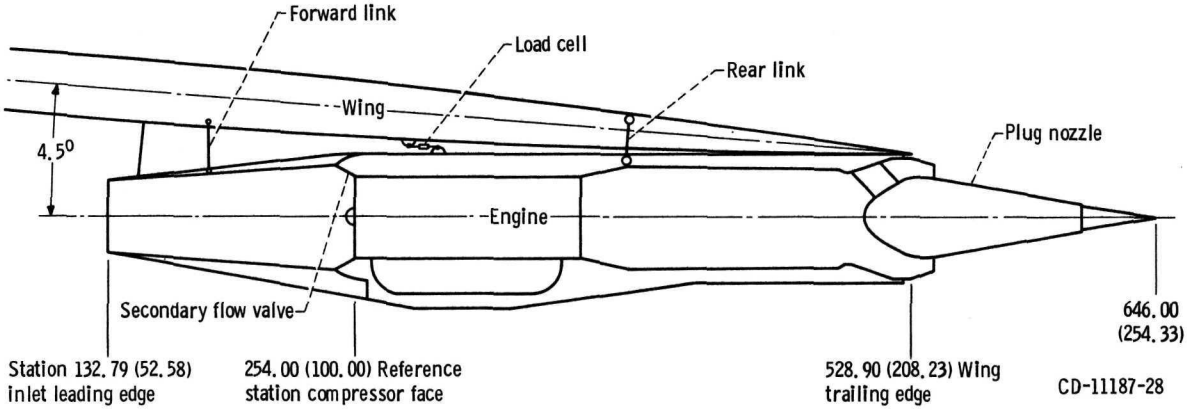

Figure 2. - Schematic of test installation. (All dimensions are in cm (in.).)

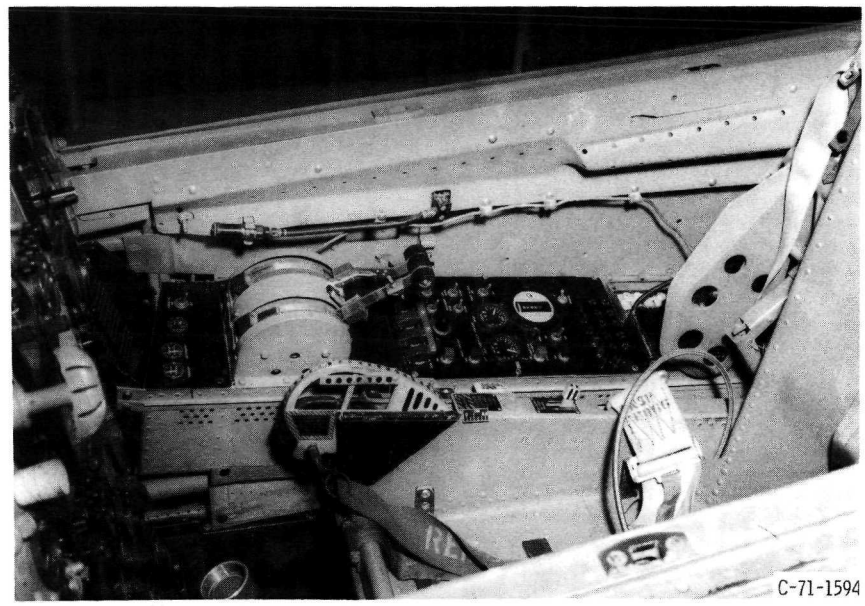

(a) J-85 dual throttle controls.

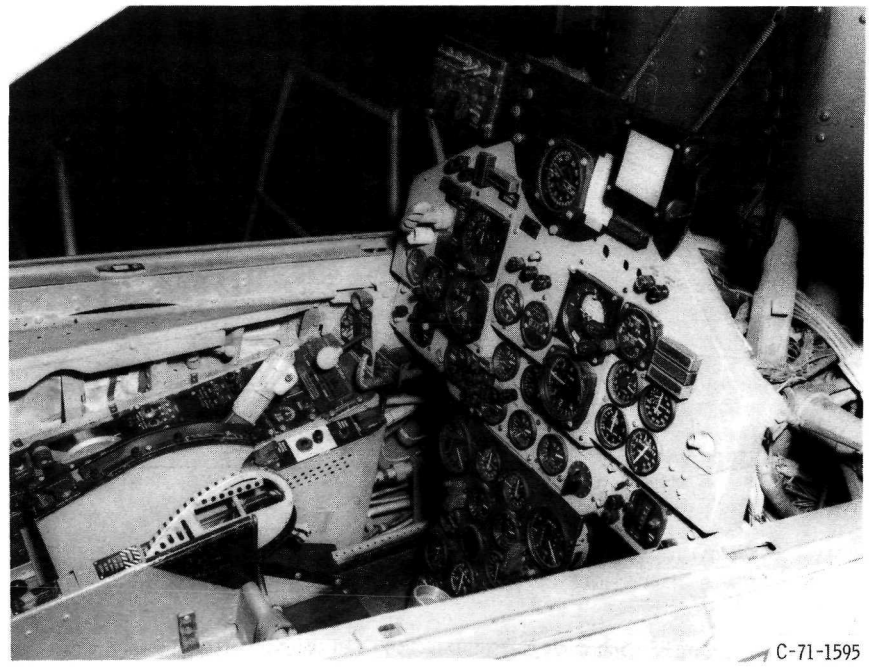

(b) Cockpit display panel.

Figure 3. - F-106B cockpit arrangement.

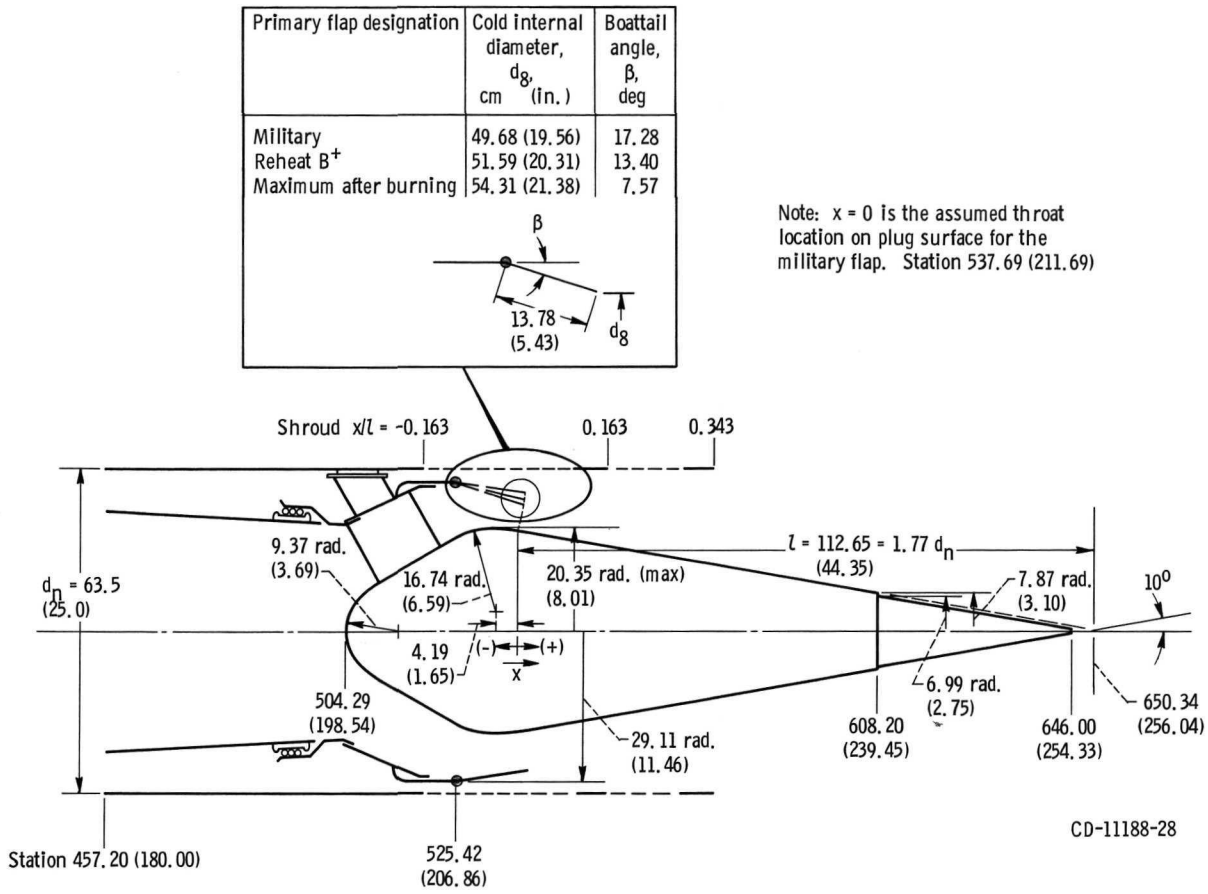

Figure 4. - Plug nozzle dimensions. (All dimensions are in cm (in.).)

Line description	Quantity	Outside diameter cm (in.)	Wall thickness, cm (in.)
Compressor bleed air	4	3.81 (1.5)	0.089 (0.035)
Strut plug and cooling air	3	2.54 (1.0)	.089 (.035)
Primary flap cooling air	6	1.91 (.75)	.089 (.035)
Distribution manifold	1	[a]9.80 by 3.81 (3.86 by 1.50)	.165 (.065)

[a]Flattened oval shape.

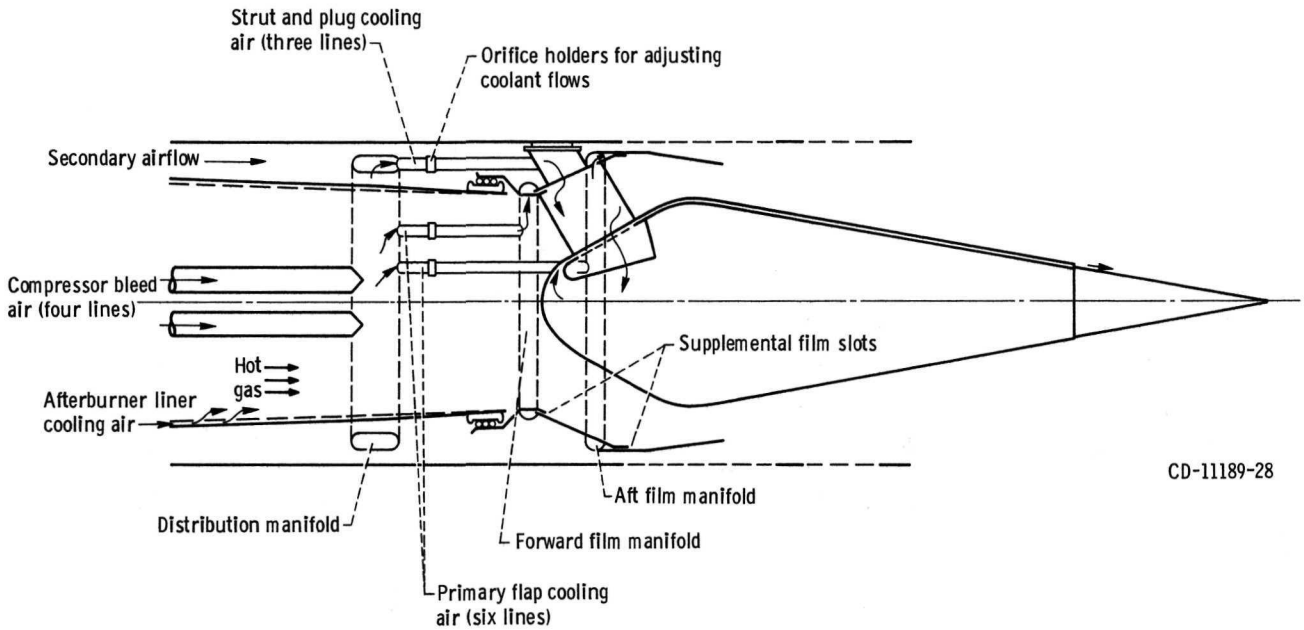

Figure 5. - Plug coolant flow paths.

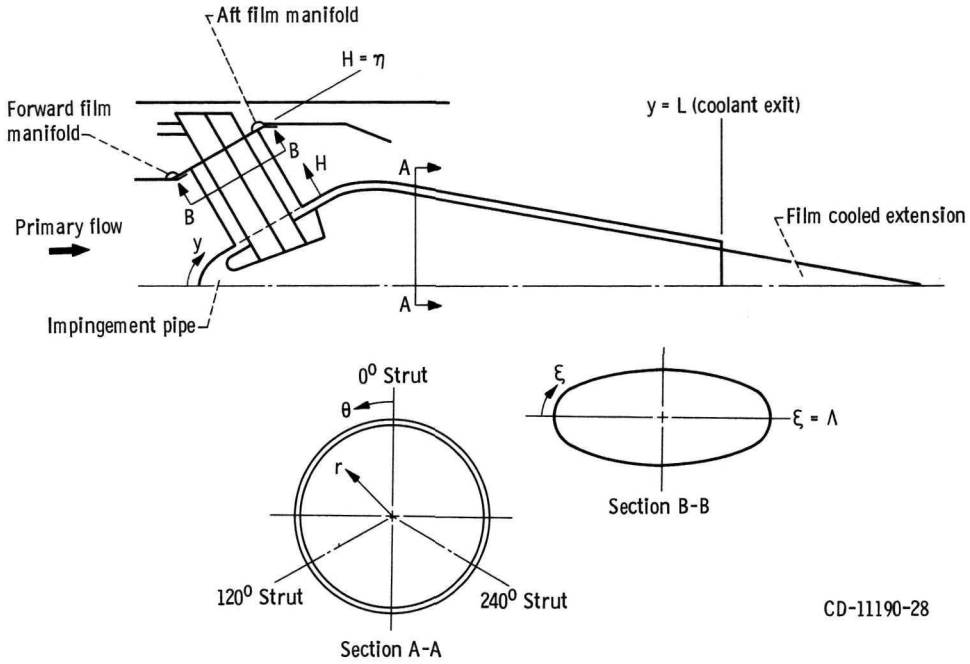

Figure 6. - Plug nozzle coordinate system used to locate instrumentation (see table I). (y Is distance along plug surface from plug front end.)

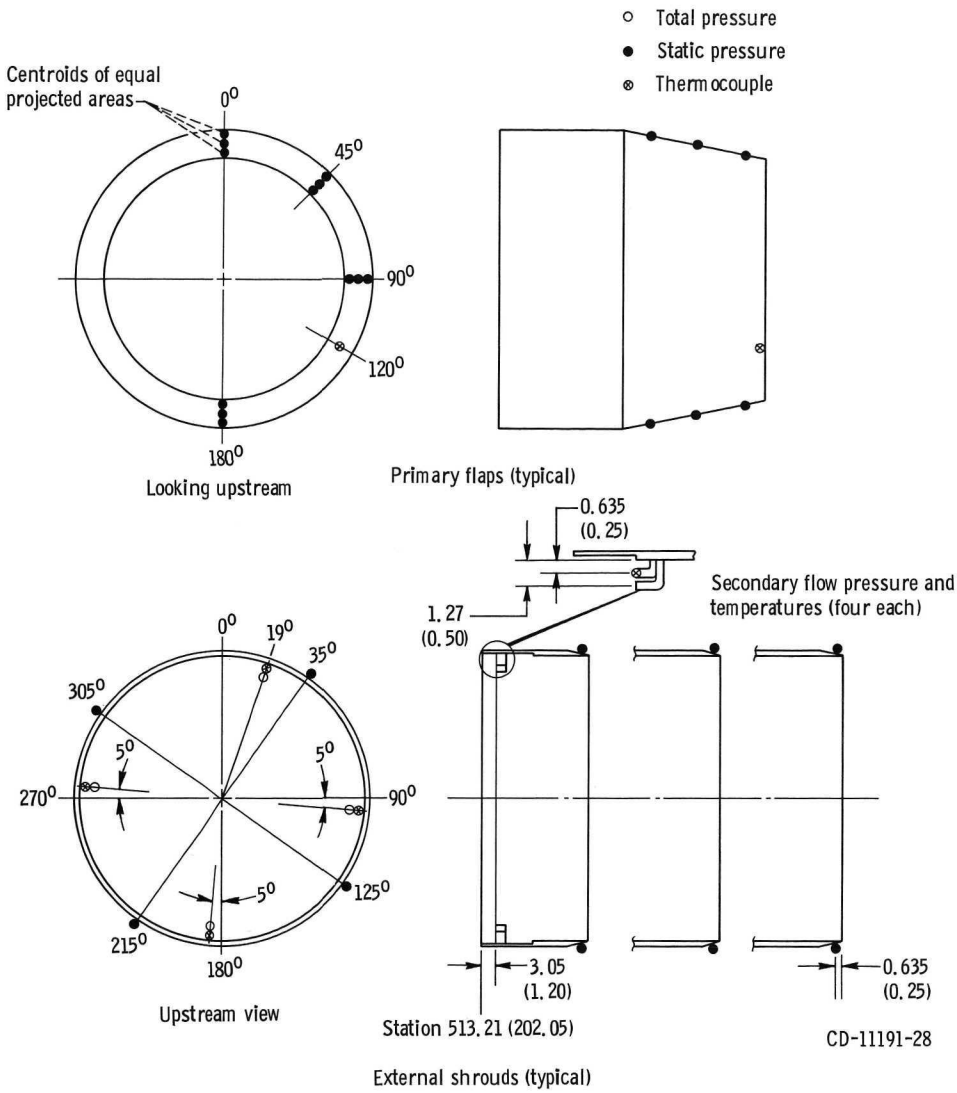

Figure 7. - Primary flap and external shroud instrumentation.

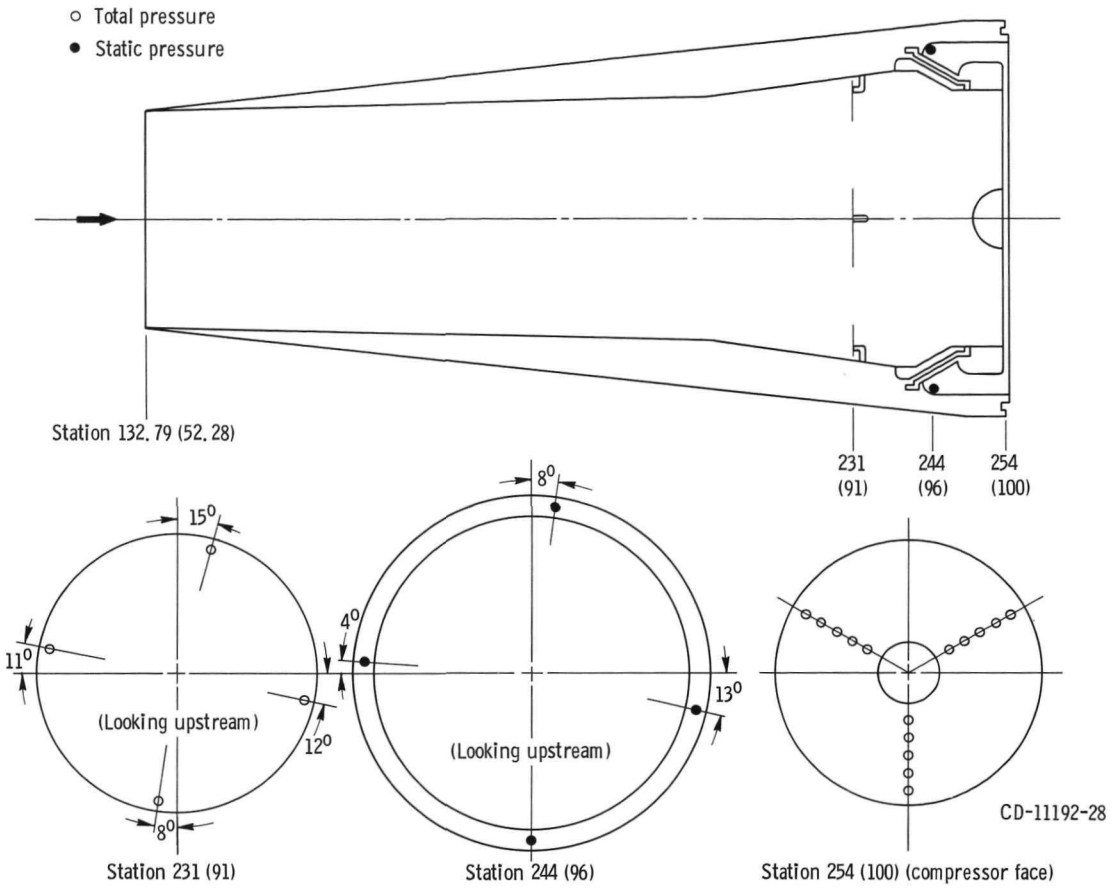

Figure 8. - Inlet and compressor face instrumentation.

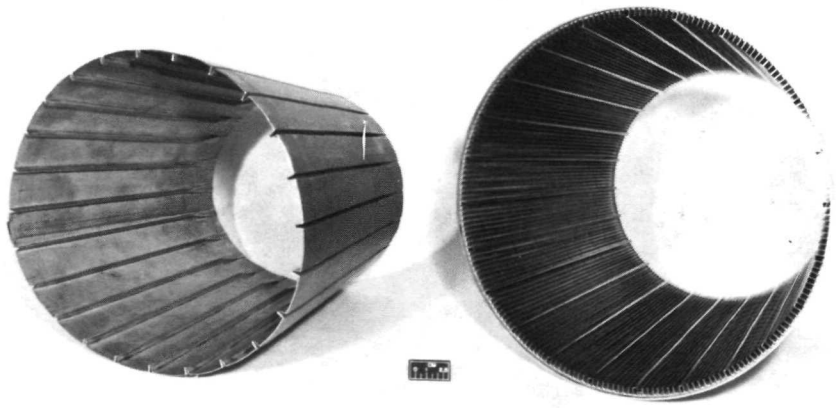

Inner wall

Outer wall with attached fins

C-68-2360

Figure 9. - Plug nozzle inner and outer wall segments.

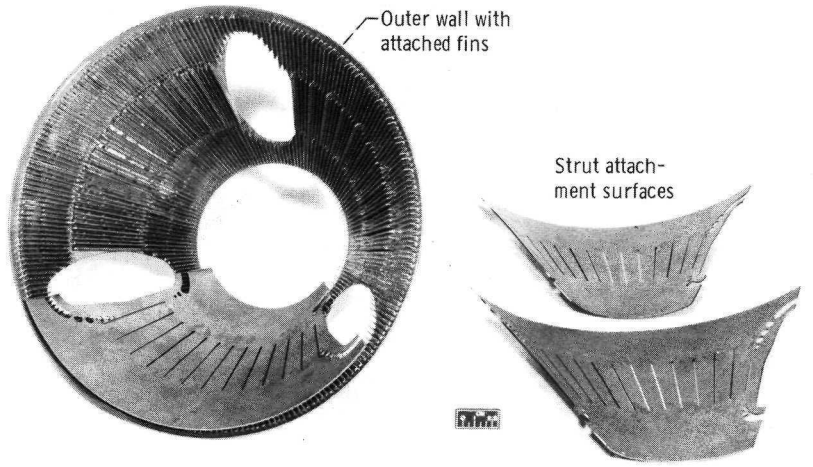

Figure 10. - Segment of plug nozzle showing strut attachment surfaces.

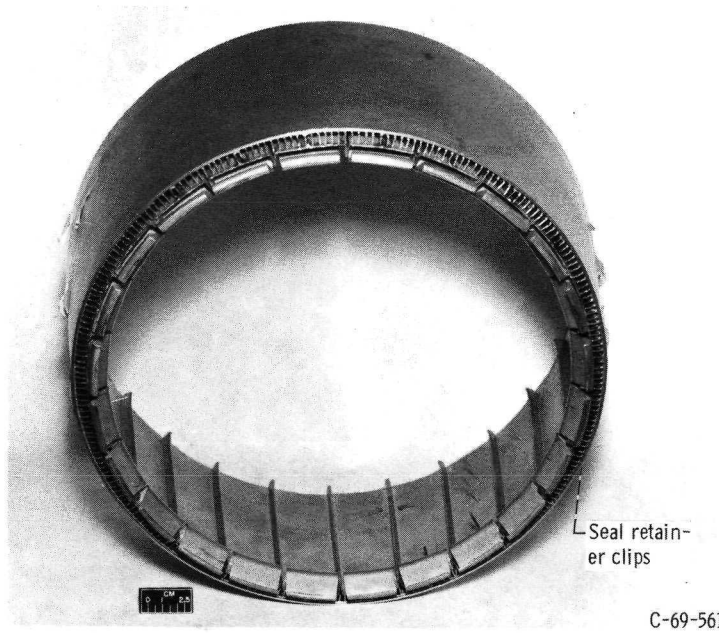

Figure 11. - Assembled plug segment showing seal retainer clips.

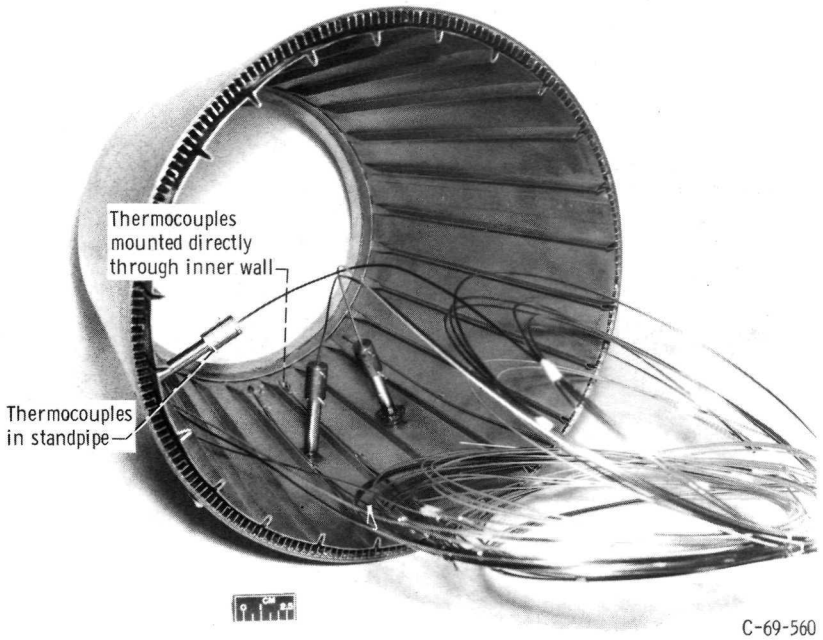

Figure 12. - Assembled plug segment showing typical thermocouple installation.

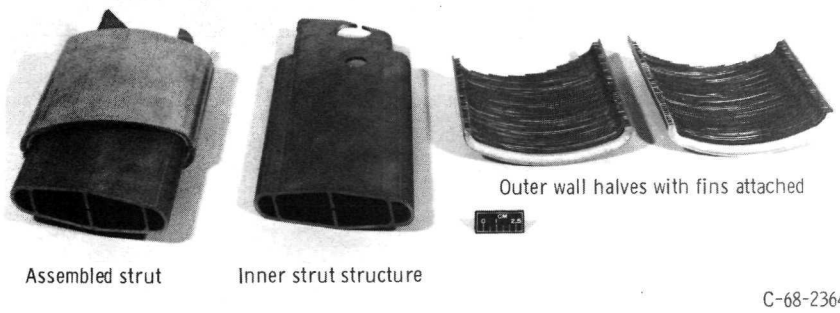

Figure 13. - Strut assembly.

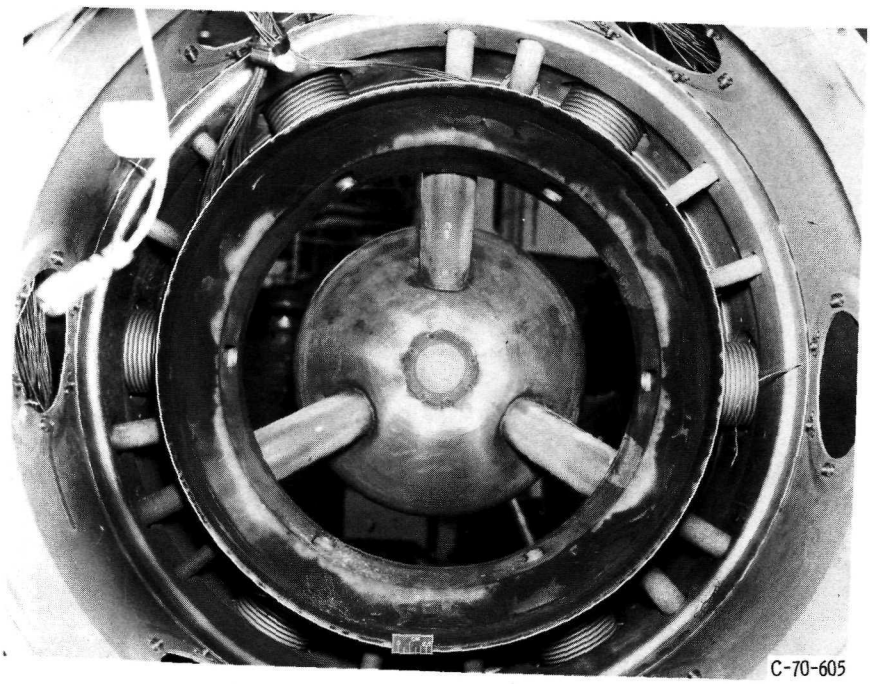

Figure 14. - Front of plug looking aft.

(a) Military primary.

(b) Reheat B^{+} primary.

Figure 15. - Installed plug nozzle.

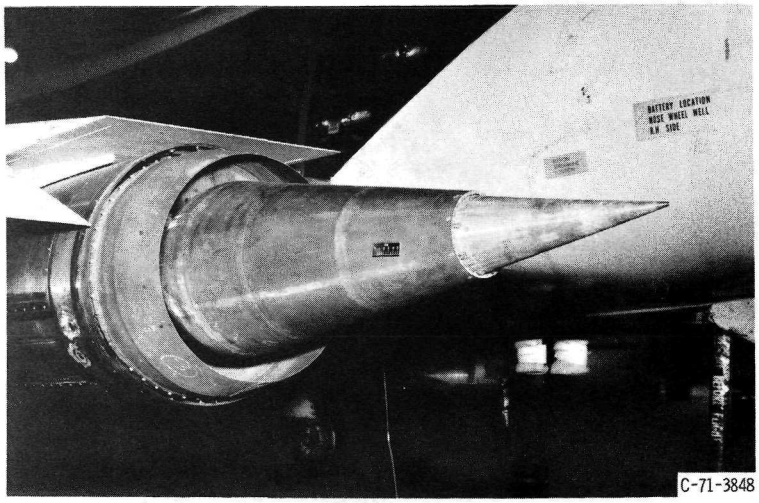

(c) Maximum afterburning primary; retracted shroud ($x/\ell = -0.163$).

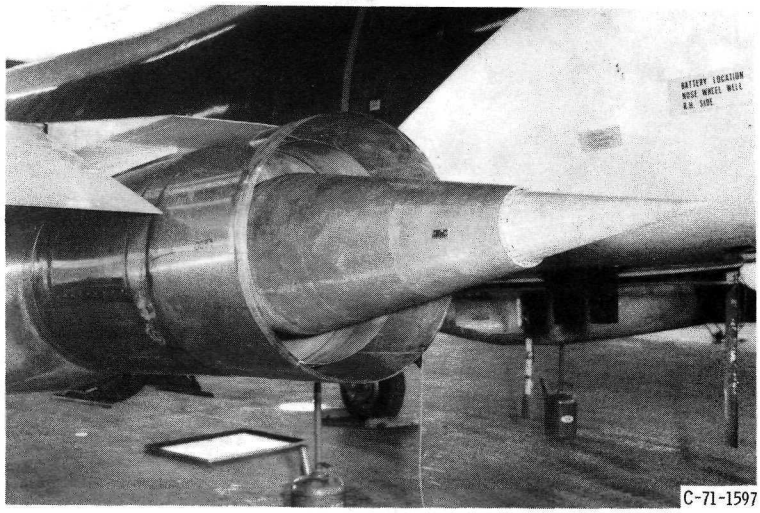

(d) Maximum afterburn primary; intermediate shroud ($x/\ell = 0.163$).

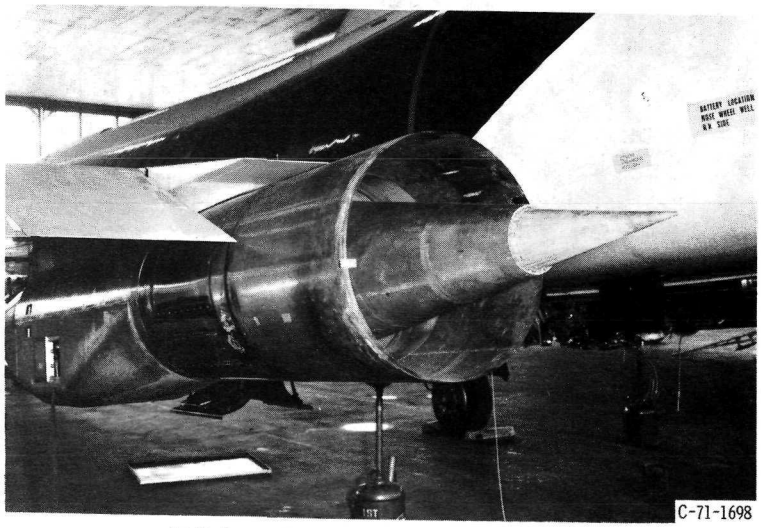

(e) Maximum afterburn primary, extended shroud ($x/\ell = 0.343$).

Figure 15. - Concluded.

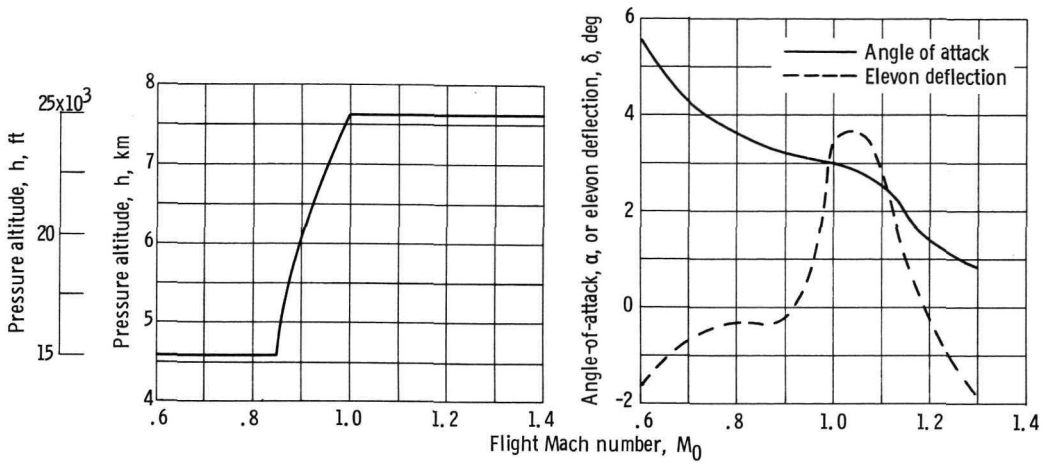

(a) Altitude variation.

(b) Angle-of-attack and elevon deflection variation.

Figure 16. - Nominal aircraft and trajectory characteristics over flight profile.

	Power setting	Nozzle effective throat area, A_{E8}, cm^2 (in.^{2})	Exhaust gas temperature, T_8, K (^{0}R)	Corrected secondary weight flow ratio, $\omega\sqrt{\tau}$	Plug coolant to primary flow ratio, ω_p	Total compressor bleed to primary flow ratio, ω_c
□	Maximum afterburning	1103 (171)	1806 (3250)	0.065	0.04	0.057
○	Reheat B$^+$	897 (139)	1444 (2600)	.032	.018	.018
◇	Military	729 (113)	956 (1720)	.032	0	0
⌀	Adjusted performance at $\omega\sqrt{\tau}$ = 0.032					
▭	Represents momentum of plug coolant based on properties at exit (station 608.20 cm (239.45 in.))					

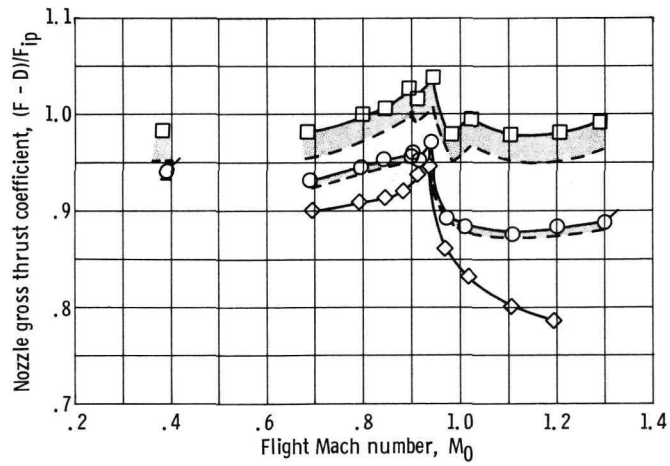

Figure 17. - Effect of power setting on performance over Mach number range. Retracted shroud (x/l = -0.163).

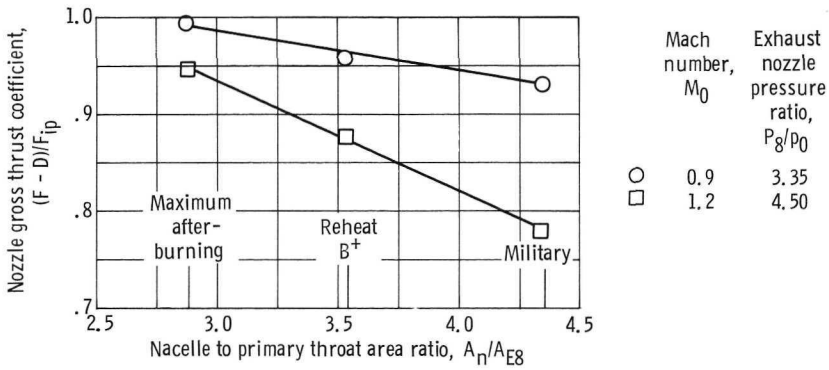

Figure 18. - Effect of primary throat area on nozzle gross thrust coefficient. Performance adjusted to corrected secondary weight flow ratio of 0.065. Coolant to primary flow ratio, $\omega_c = \omega_p$, 0; retracted shroud (x/ℓ = -0.163). (See table II.)

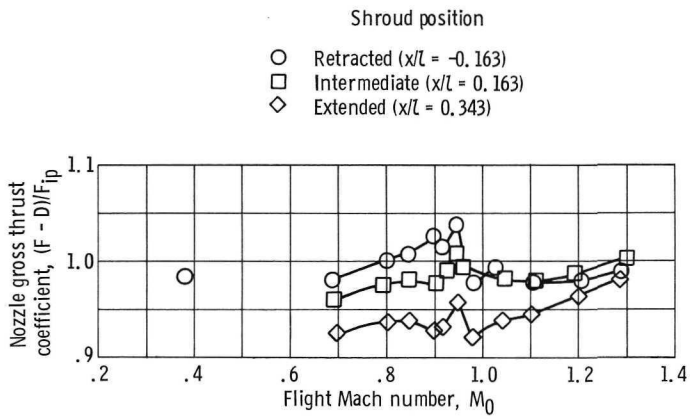

Figure 19. - Effect of shroud extension on performance at maximum afterburning power over Mach number range. Corrected secondary weight flow, 0.065; total compressor bleed to primary flow ratio, 0.058; plug coolant to primary flow ratio, 0.04.

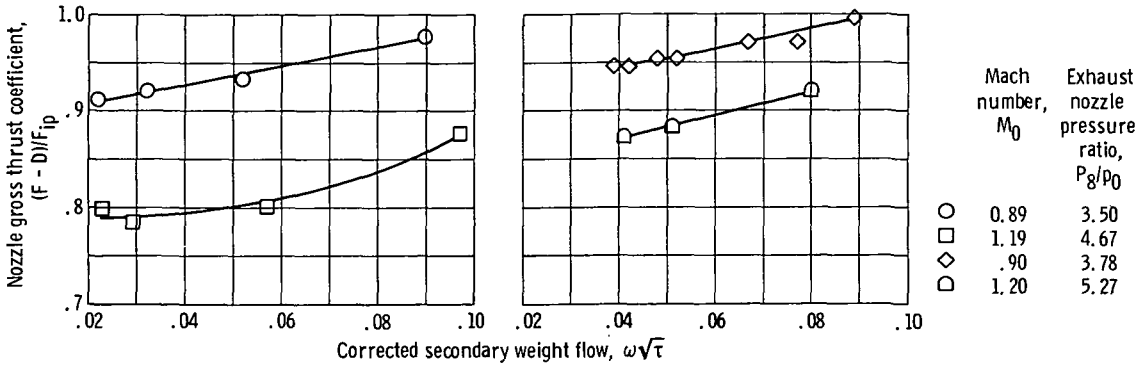

(a) Military power; nozzle effective throat area, 729 square centimeters (113 in.^{2}); exhaust gas temperature, 956 K (1720^0 R); coolant to primary flow ratio, $\omega_c = \omega_p = 0$.

(b) Reheat B$^+$; nozzle effective throat area, 897 square centimeters (139 in.^{2}); exhaust temperature, 1444 K (2600^0 R); coolant to primary flow ratio, $\omega_c = \omega_p = 0.018$.

Figure 20. - Effect of secondary weight flow on performance at nominal Mach numbers of 0.9 and 1.2. Retracted shroud ($x/l = -0.163$).

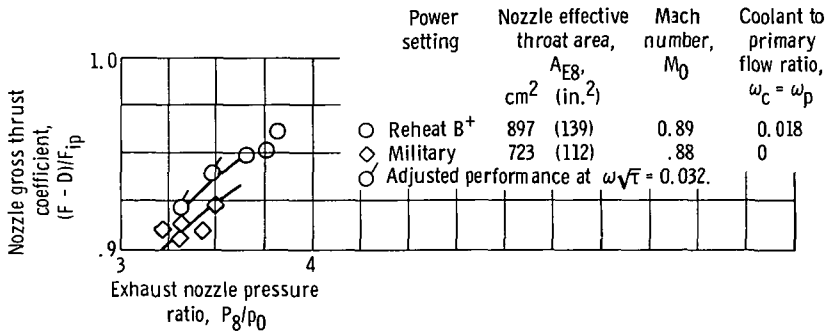

Figure 21. - Effect of exhaust nozzle pressure ratio on performance with military and reheat B$^+$ primary flaps, a nominal Mach number, M_0 of 0.9 and a corrected secondary weight flow of 0.032. Retracted shroud ($x/l = -0.163$).

Figure 22. - Engine and coolant flow conditions.

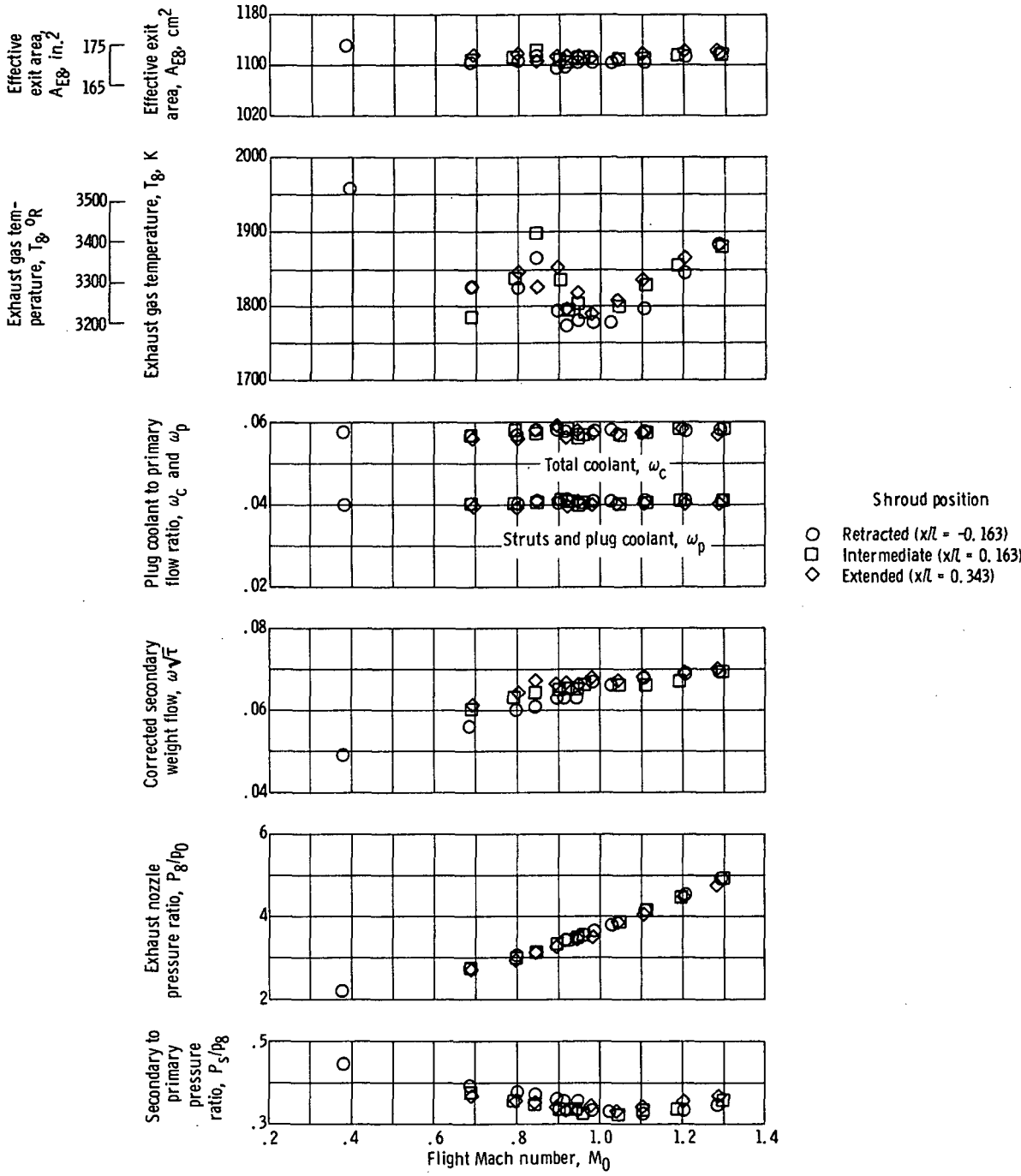

(c) Maximum afterburning for various shroud positions.

Figure 22. - Concluded.

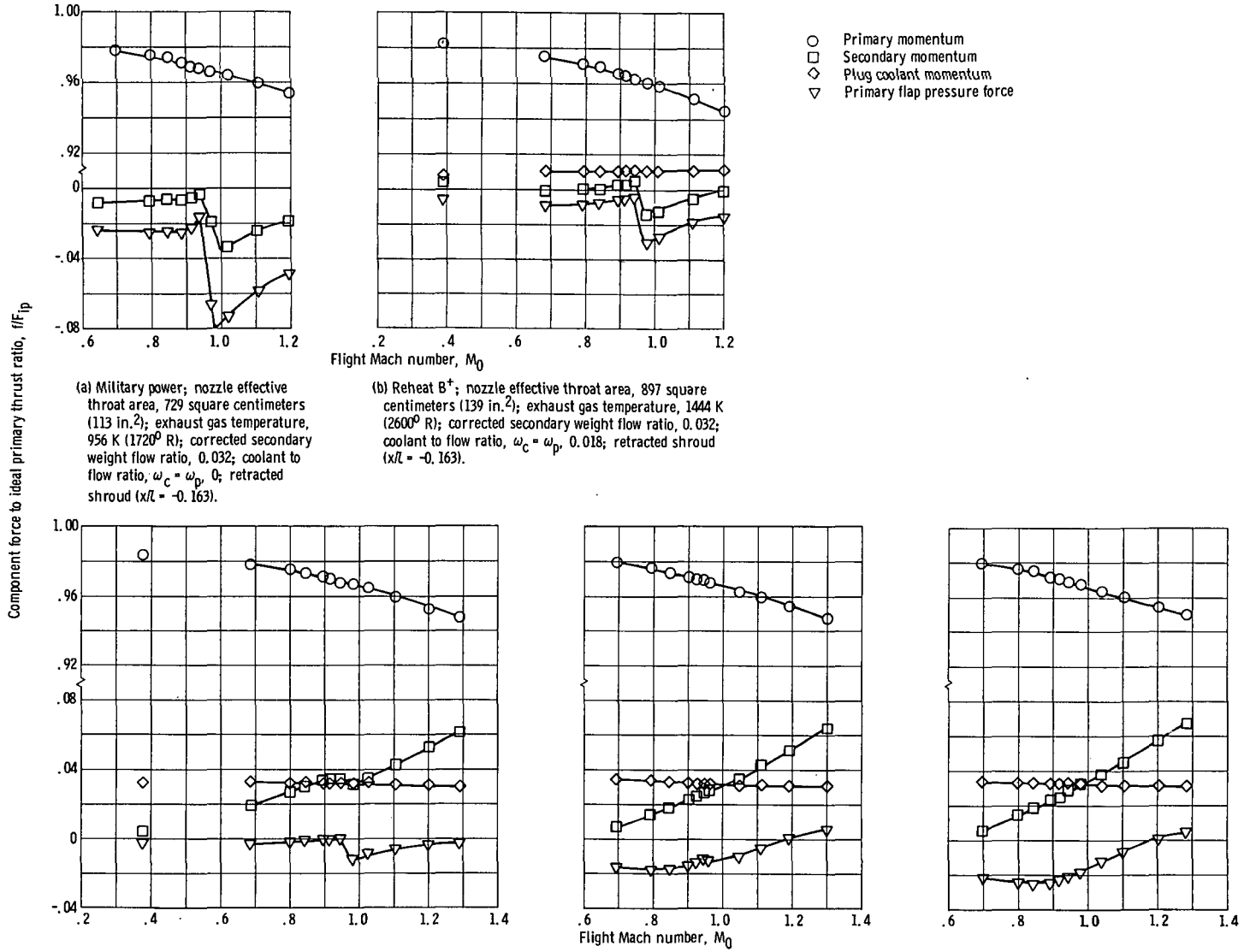

(a) Military power; nozzle effective throat area, 729 square centimeters (113 in.^{2}); exhaust gas temperature, 956 K (1720^0 R); corrected secondary weight flow ratio, 0.032; coolant to flow ratio, $\omega_c = \omega_p$, 0; retracted shroud ($x/\ell = -0.163$).

(b) Reheat B$^+$; nozzle effective throat area, 897 square centimeters (139 in.^{2}); exhaust gas temperature, 1444 K (2600^0 R); corrected secondary weight flow ratio, 0.032; coolant to flow ratio, $\omega_c = \omega_p$, 0.018; retracted shroud ($x/\ell = -0.163$).

(c) Maximum afterburning; nozzle effective throat area, 1103 square centimeters (171 in.^{2}); exhaust gas temperature, 1833 K (3300^0 R); corrected secondary weight flow ratio, 0.065; total coolant to primary flow ratio, 0.058; plug coolant to primary flow ratio, 0.041; retracted shroud ($x/\ell = -0.163$).

(d) Maximum afterburning; nozzle effective throat area, 1103 square centimeters (171 in.^{2}); exhaust gas temperature, 1833 K (3300^0 R); corrected secondary weight flow ratio, 0.066; total coolant to primary flow ratio, 0.058; plug coolant to primary flow ratio, 0.041; intermediate shroud ($x/\ell = 0.163$).

(e) Maximum afterburning; nozzle effective throat area, 1103 square centimeters (171 in.^{2}); exhaust gas temperature, 1833 K (3300^0 R); corrected secondary weight flow ratio, 0.067; total coolant to primary flow ratio, 0.058; plug coolant to primary flow ratio, 0.041; extended shroud ($x/\ell = 0.343$).

Figure 23. - Plug nozzle component forces over Mach number range.

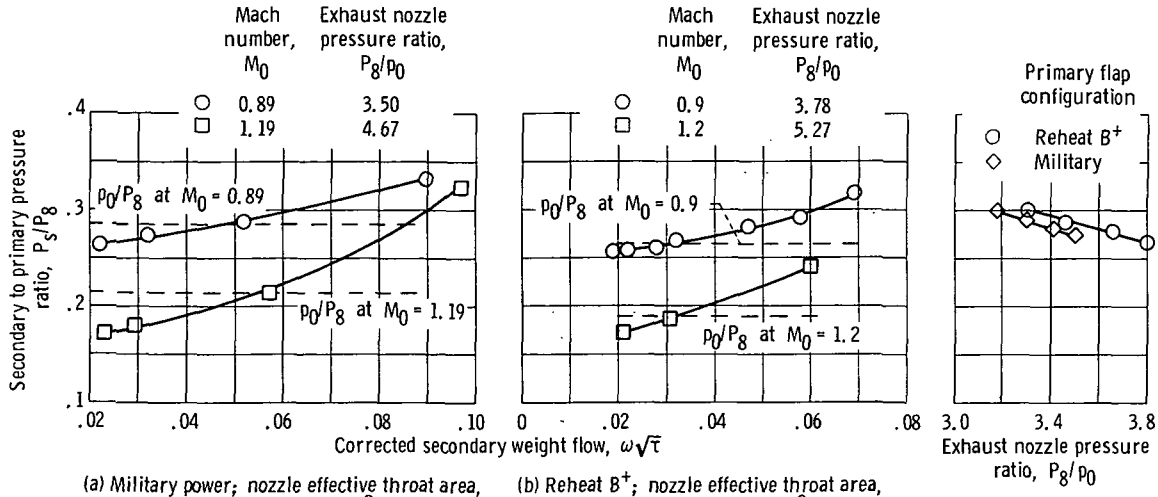

(a) Military power; nozzle effective throat area, 729 square centimeters (113 in.^{2}); exhaust gas temperature, 956 K (1720^0 R); coolant to primary flow ratio, $\omega_c = \omega_p$, 0; retracted shroud, (x/ℓ = -0.163).

(b) Reheat B^+; nozzle effective throat area, 897 square centimeters (139 in.^{2}); exhaust gas temperature, 1444 K (2600^0 R); coolant to primary flow ratio, $\omega_c = \omega_p$, 0.018; retracted shroud (x/ℓ = -0.163).

(c) Mach 0.90; corrected secondary weight flow ratio, 0.033; retracted shroud (x/ℓ = -0.163).

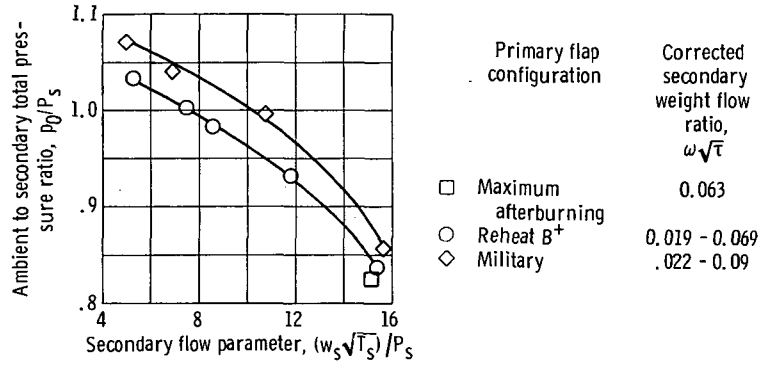

(d) Mach 0.90; retracted shroud (x/ℓ = -0.163).

Figure 24. - Pumping characteristics.

	Static values	Flight values
Exhaust gas temperature, T_8, K (^oR)	1680 (3025)	1794 (3230)
Exhaust gas pressure, P_8, atm	1.78	1.57
Exhaust gas weight flow, w_8, kg/sec (lbm/sec)	18.95 (41.78)	15.65 (34.52)
Exhaust nozzle pressure ratio, P_8/p_0	3.32	3.37
Corrected secondary weight flow ratio, $\omega\sqrt{\tau}$	0.052	0.063
Plug coolant to primary flow ratio, ω_p	0.035	0.040
Mach number, M_0	-----	0.90

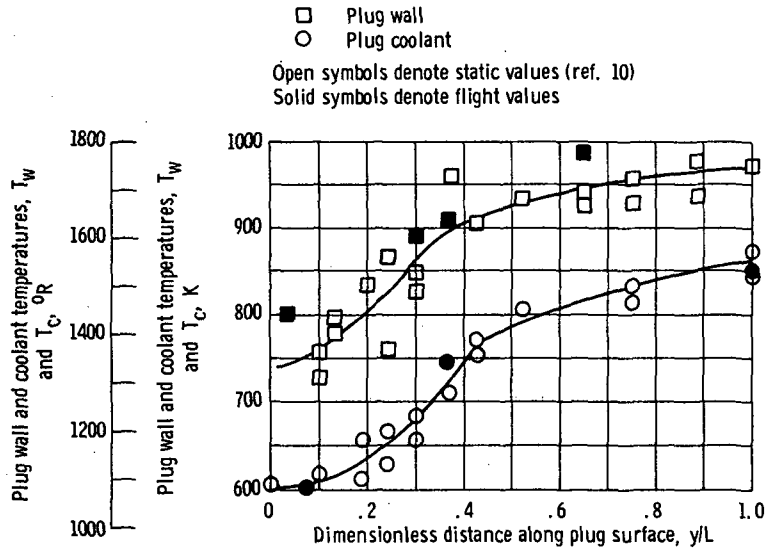

Figure 25. - Coolant and plug wall temperature variations - static and flight data. Maximum afterburning configuration; retracted shroud (x/L = -0.163).

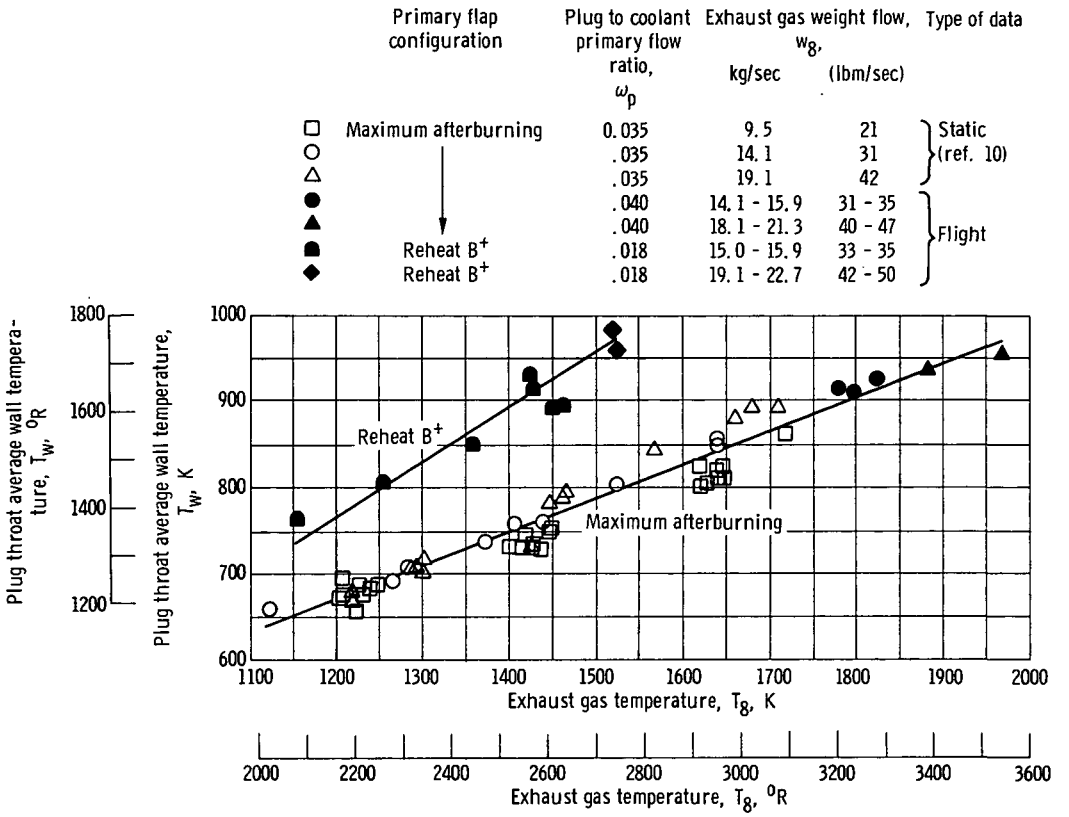

Figure 26. - Effect of exhaust gas temperature on plug throat wall temperature - static and flight data, retracted shroud (x/ℓ = -0.163).

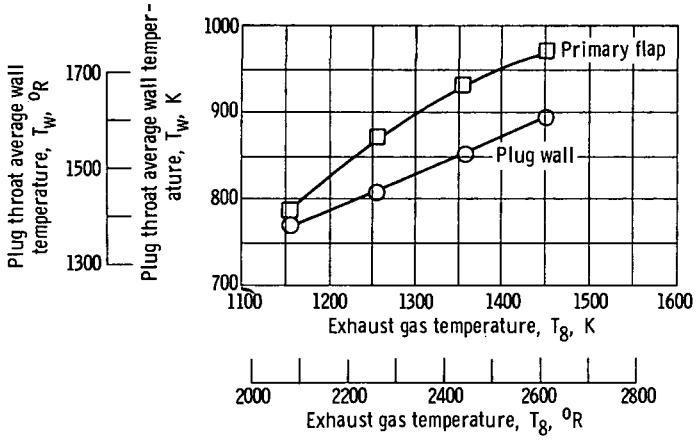

Figure 27. - Effect of exhaust gas temperature on throat wall temperature. Mach 0.9; corrected secondary weight flow ratio, 0.033; coolant to primary flow ratio, $\omega_c = \omega_p$, 0.018; nozzle effective throat area, 897 square centimeters (139 in.^{2}); exhaust nozzle pressure ratio, 3.29 to 3.81; reheat B$^+$ primary flap; retracted shroud (x/ℓ = -0.163).

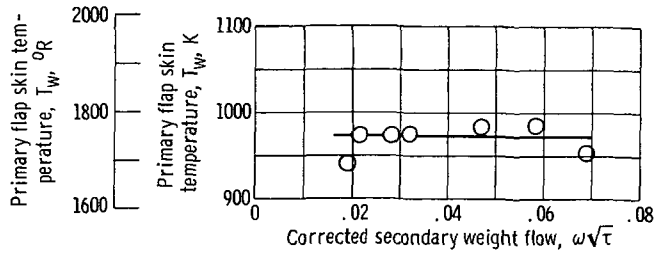

Figure 28. - Effect of secondary weight flow on primary flap skin temperature. Reheat B^+; nozzle effective throat area, 897 square centimeters (139 $in.^2$); exhaust gas temperature, 1444 K (2600^o R); Mach 0.9; retracted shroud (x/ℓ = -0.163).

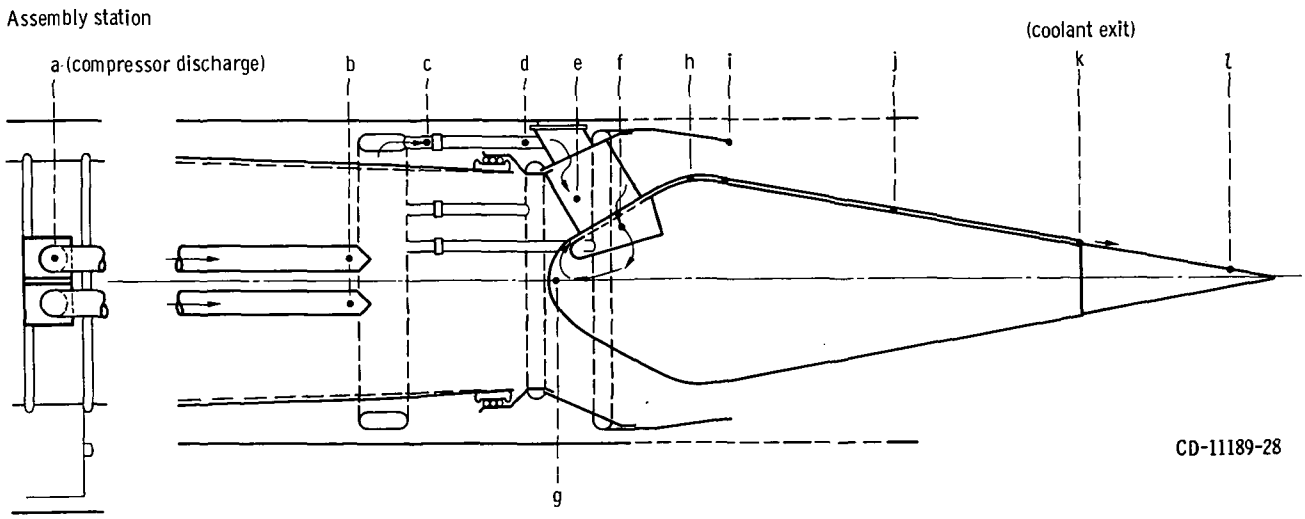

Figure 29. - Plug coolant flow path and measuring stations.

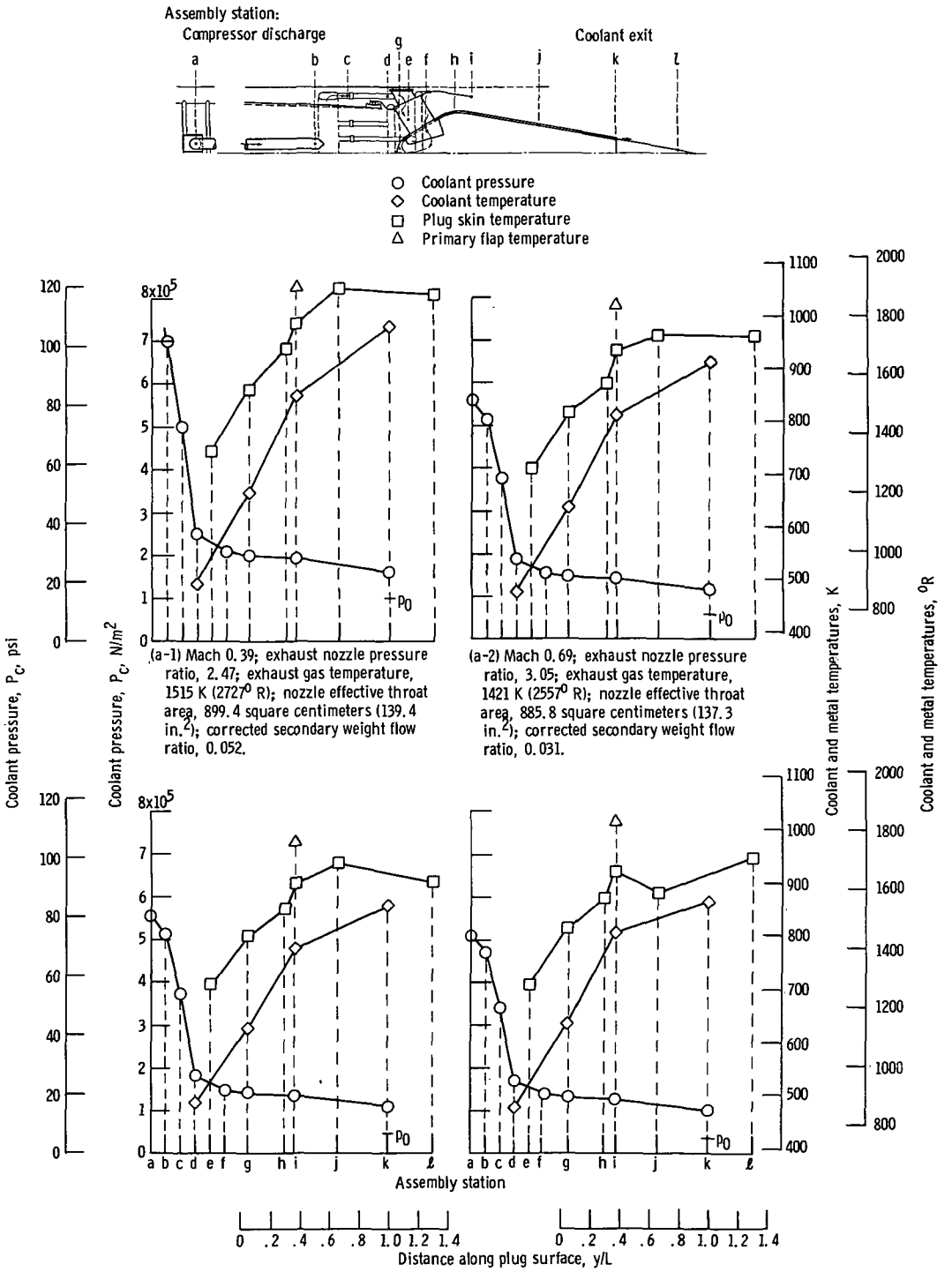

(a-1) Mach 0.39; exhaust nozzle pressure ratio, 2.47; exhaust gas temperature, 1515 K (2727^0 R); nozzle effective throat area, 899.4 square centimeters (139.4 in.^{2}); corrected secondary weight flow ratio, 0.052.

(a-2) Mach 0.69; exhaust nozzle pressure ratio, 3.05; exhaust gas temperature, 1421 K (2557^0 R); nozzle effective throat area, 885.8 square centimeters (137.3 in.^{2}); corrected secondary weight flow ratio, 0.031.

(a-3) Mach 0.89; exhaust nozzle pressure ratio, 3.75; exhaust gas temperature, 1462 K (2631^0 R); nozzle effective throat area, 885.2 square centimeters (137.2 in.^{2}); corrected secondary weight flow ratio, 0.032.

(a-4) Mach 1.01; exhaust nozzle pressure ratio, 4.27; exhaust gas temperature, 1426 K (2567^0 R); nozzle effective throat area, 883.9 square centimeters (137.0 in.^{2}); corrected secondary weight flow ratio, 0.031.

(a) Reheat B$^+$; coolant to primary flow ratio, $\omega_c = \omega_p$, 0.018; retracted shroud (x/ℓ = -0.163).

Figure 30. - Coolant characteristics and metal temperatures.

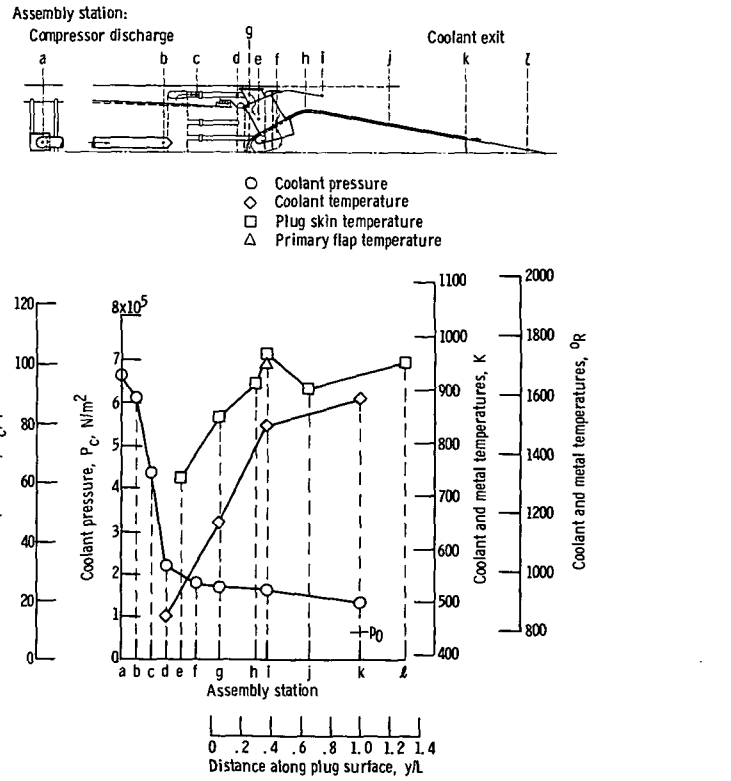

(a-5) Mach 1.30; exhaust nozzle pressure ratio, 5.81; exhaust gas temperature, 1521 K (2737^0 R); nozzle effective throat area, 882.5 square centimeters (136.8 in.^{2}); corrected secondary weight flow ratio, 0.059.

(a) Concluded.

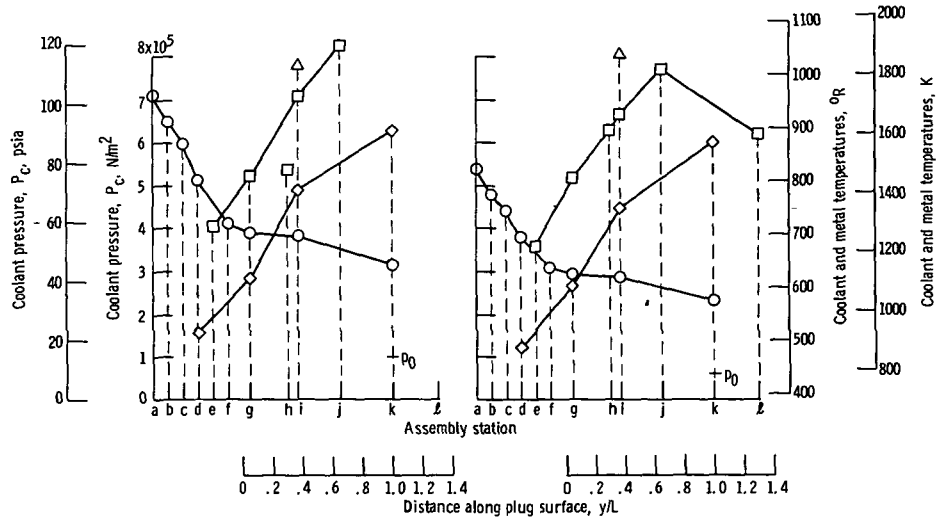

(b-1) Mach 0.38; exhaust nozzle pressure ratio, 2.23; exhaust gas temperature, 1967 K (3540^0 R); nozzle effective throat area, 1130.3 square centimeters (175.2 in.^{2}); corrected secondary weight flow ratio, 0.049; total coolant to primary flow ratio, 0.058; plug coolant to primary flow ratio, 0.04.

(b-2) Mach 0.69; exhaust nozzle pressure ratio, 2.79; exhaust gas temperature, 1824 K (3283^0 R); nozzle effective throat area, 1101.3 square centimeters (170.7 in.^{2}); corrected secondary weight flow ratio, 0.056; total coolant to primary flow ratio, 0.057; plug coolant to primary flow ratio, 0.040.

(b) Maximum afterburning; retracted shroud (x/ℓ = -0.163).

Figure 30. - Continued.

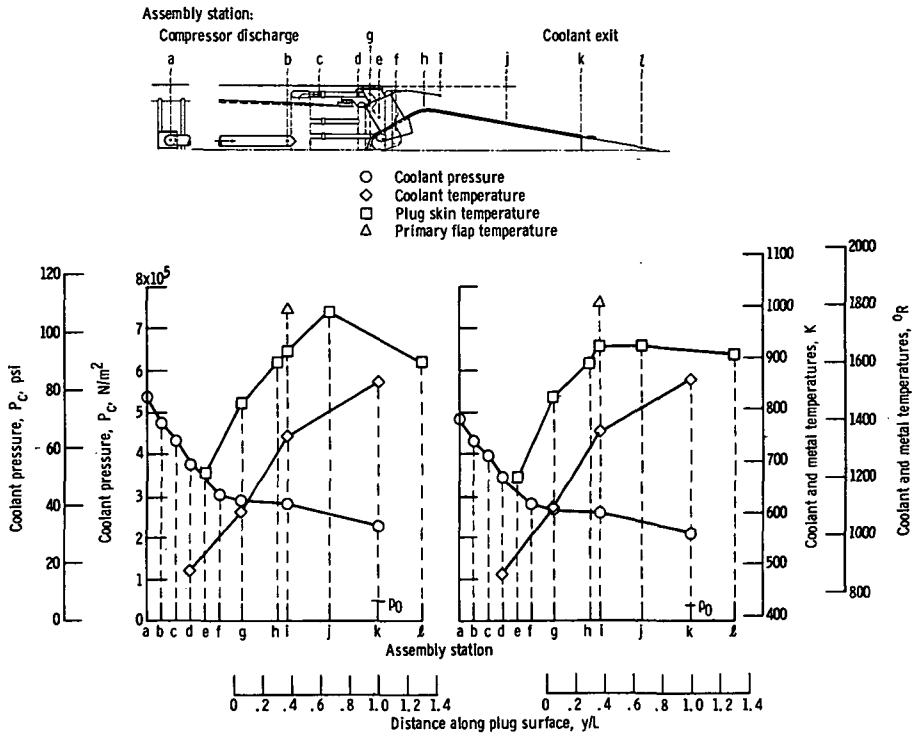

(b-3) Mach 0.90; exhaust nozzle pressure ratio, 3.37; exhaust gas temperature, 1794 K (3230° R); nozzle effective throat area, 1091.6 square centimeters (169.2 in.^{2}); corrected secondary weight flow ratio, 0.063; total coolant to primary flow ratio, 0.058; plug coolant to primary flow ratio, 0.040.

(b-4) Mach 0.98; exhaust nozzle pressure ratio, 3.64; exhaust gas temperature, 1780 K (3204° R); nozzle effective throat area, 1101.9 square centimeters (170.8 in.^{2}); corrected secondary weight flow ratio, 0.067; total coolant to primary flow ratio, 0.058; plug coolant to primary flow ratio, 0.041.

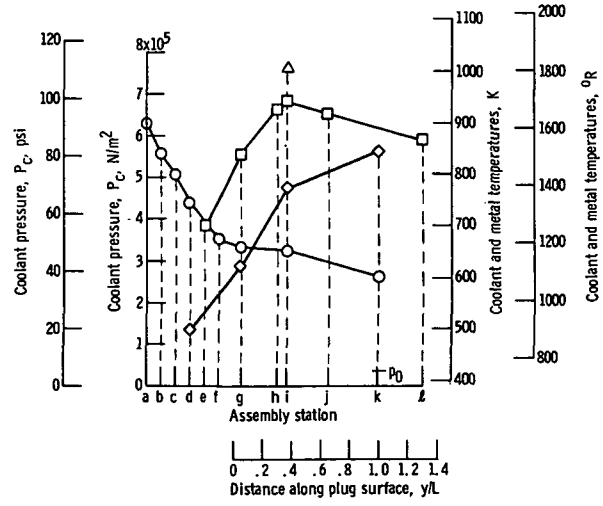

(b-5) Mach 1.29; exhaust nozzle pressure ratio, 4.91; exhaust gas temperature, 1884 K (3391° R); nozzle effective throat area, 1116.8 square centimeters (173.1 in.^{2}); corrected secondary weight flow ratio, 0.069; total coolant to primary flow ratio, 0.058; plug coolant to primary flow ratio, 0.041.

(b) Concluded.

Figure 30. - Continued.

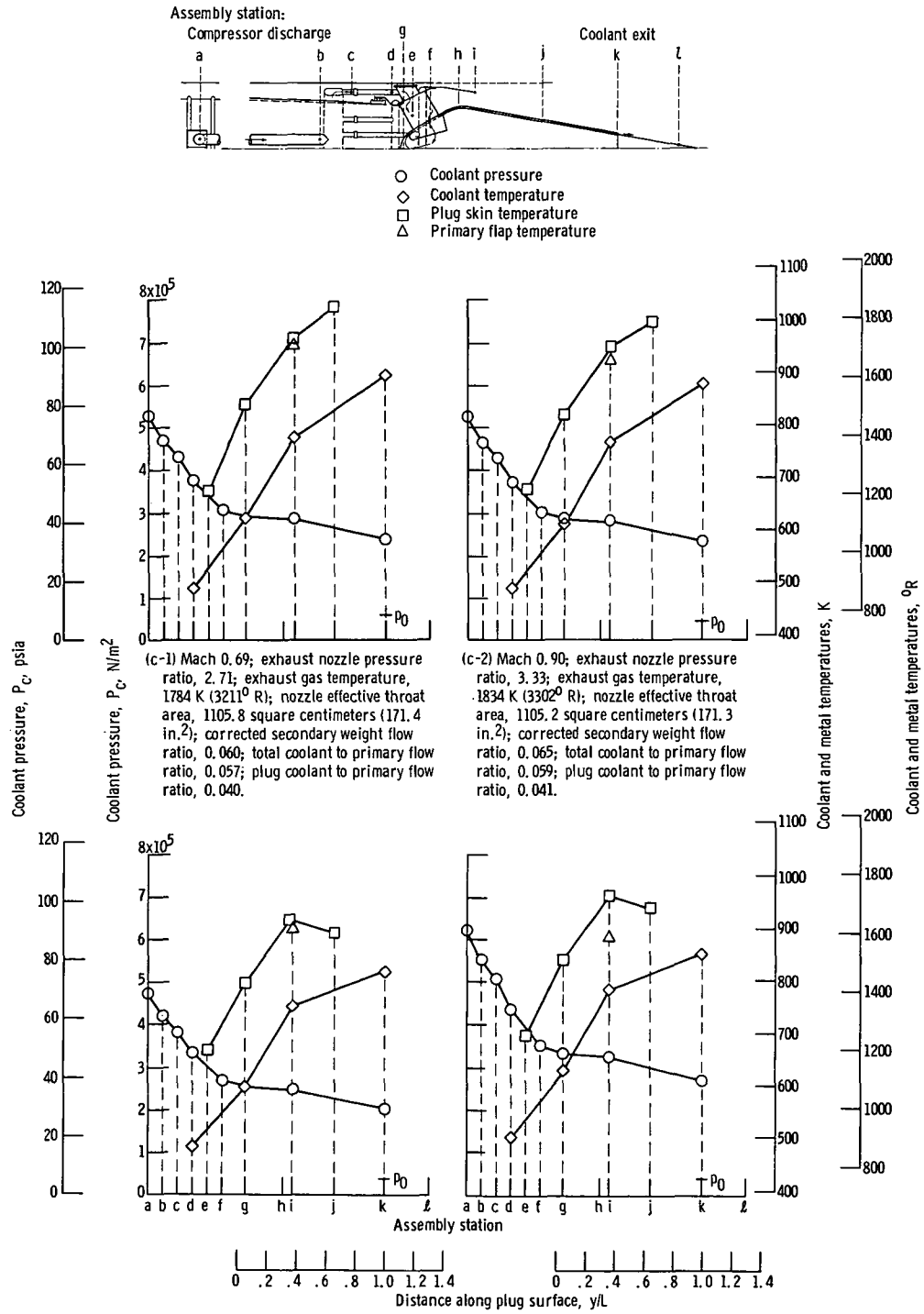

(c-1) Mach 0.69; exhaust nozzle pressure ratio, 2.71; exhaust gas temperature, 1784 K (3211° R); nozzle effective throat area, 1105.8 square centimeters (171.4 in.^{2}); corrected secondary weight flow ratio, 0.060; total coolant to primary flow ratio, 0.057; plug coolant to primary flow ratio, 0.040.

(c-2) Mach 0.90; exhaust nozzle pressure ratio, 3.33; exhaust gas temperature, 1834 K (3302° R); nozzle effective throat area, 1105.2 square centimeters (171.3 in.^{2}); corrected secondary weight flow ratio, 0.065; total coolant to primary flow ratio, 0.059; plug coolant to primary flow ratio, 0.041.

(c-3) Mach 1.04; exhaust nozzle pressure ratio, 3.86; exhaust gas temperature, 1799 K (3239° R); nozzle effective throat area, 1103.2 square centimeters (171.0 in.^{2}); corrected secondary weight flow ratio, 0.066; total coolant to primary flow ratio, 0.057; plug coolant to primary flow ratio, 0.040.

(c-4) Mach 1.30; exhaust nozzle pressure ratio, 4.91; exhaust gas temperature, 1882 K (3387° R); nozzle effective throat area, 1112.9 square centimeters (172.5 in.^{2}); corrected secondary weight flow ratio, 0.069; total coolant to primary flow ratio, 0.058; plug coolant to primary flow ratio, 0.041.

(c) Maximum afterburning; intermediate shroud (x/ℓ = 0.163).

Figure 30. - Continued.

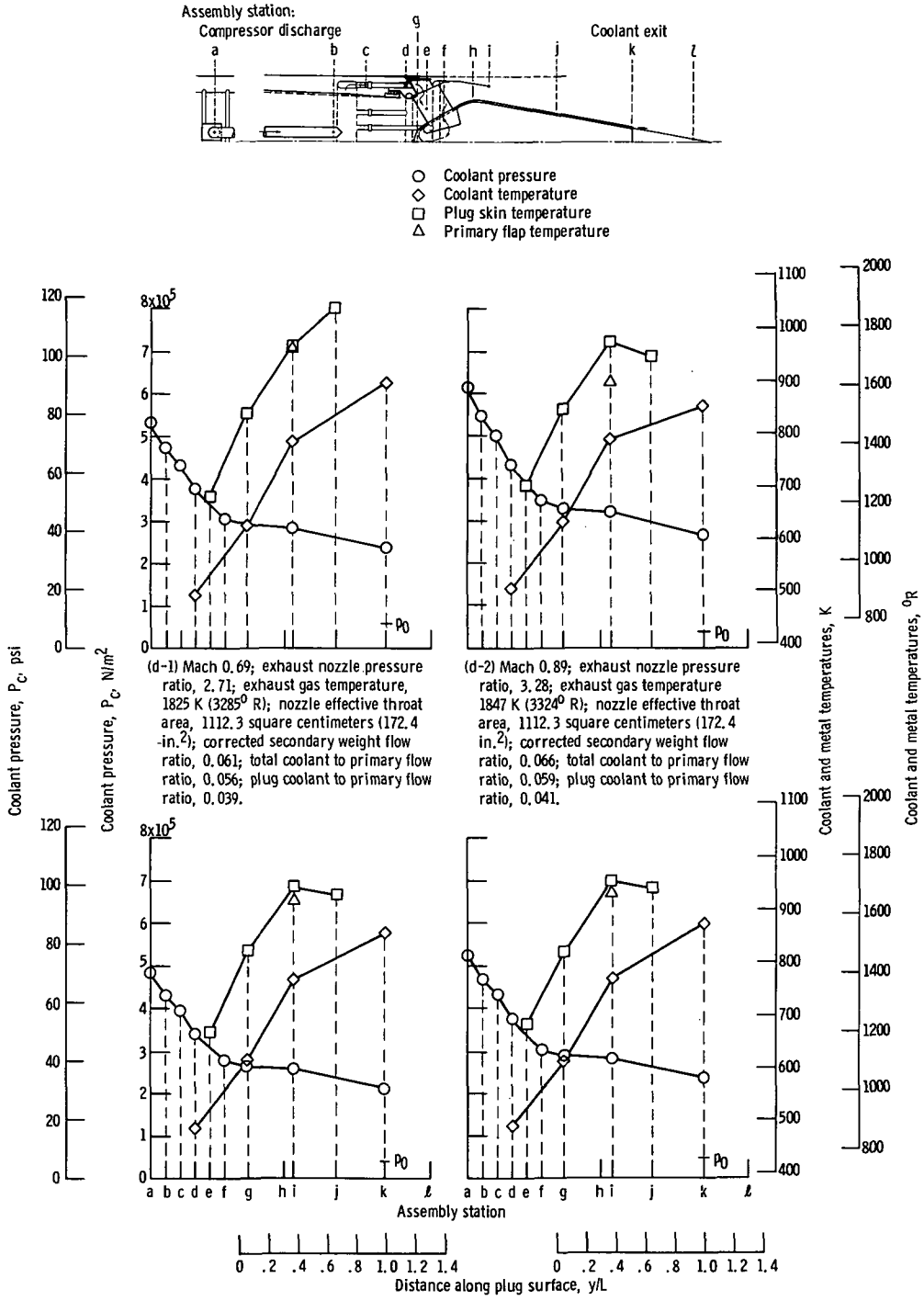

(d-1) Mach 0.69; exhaust nozzle pressure ratio, 2.71; exhaust gas temperature, 1825 K (3285^0 R); nozzle effective throat area, 1112.3 square centimeters (172.4 in.^{2}); corrected secondary weight flow ratio, 0.061; total coolant to primary flow ratio, 0.056; plug coolant to primary flow ratio, 0.039.

(d-2) Mach 0.89; exhaust nozzle pressure ratio, 3.28; exhaust gas temperature 1847 K (3324^0 R); nozzle effective throat area, 1112.3 square centimeters (172.4 in.^{2}); corrected secondary weight flow ratio, 0.066; total coolant to primary flow ratio, 0.059; plug coolant to primary flow ratio, 0.041.

(d-3) Mach 0.98; exhaust nozzle pressure ratio, 3.55; exhaust gas temperature, 1789 K (3220^0 R); nozzle effective throat area, 1106.4 square centimeters (171.5 in.^{2}); corrected secondary weight flow ratio, 0.068; total coolant to primary flow ratio, 0.057; plug coolant to primary flow ratio, 0.040.

(d-4) Mach 1.28; exhaust nozzle pressure ratio, 4.78; exhaust gas temperature, 1882 K (3387^0 R); nozzle effective throat area, 1120.0 square centimeters (173.6 in.^{2}); corrected secondary weight flow ratio, 0.070; total coolant to primary flow ratio, 0.057; plug coolant to primary flow ratio, 0.040.

(d) Maximum afterburning; extended shroud (x/L = 0.343).

Figure 30. - Concluded.

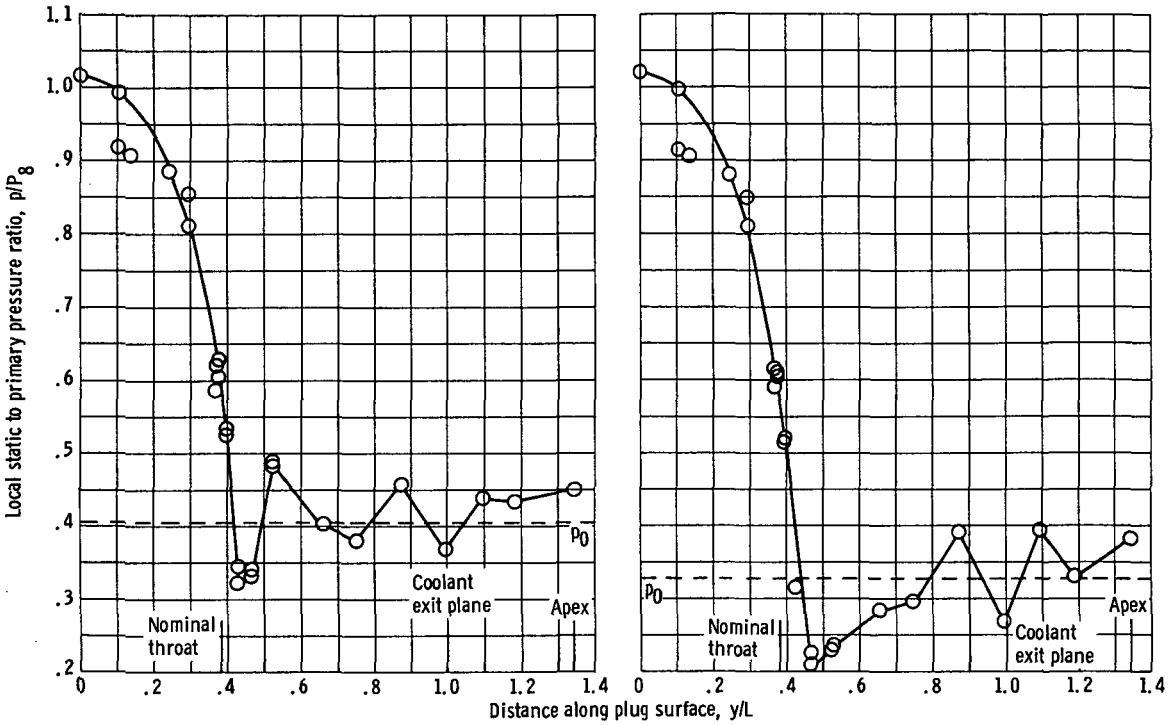

(a-1) Mach 0.39.

(a-2) Mach 0.69.

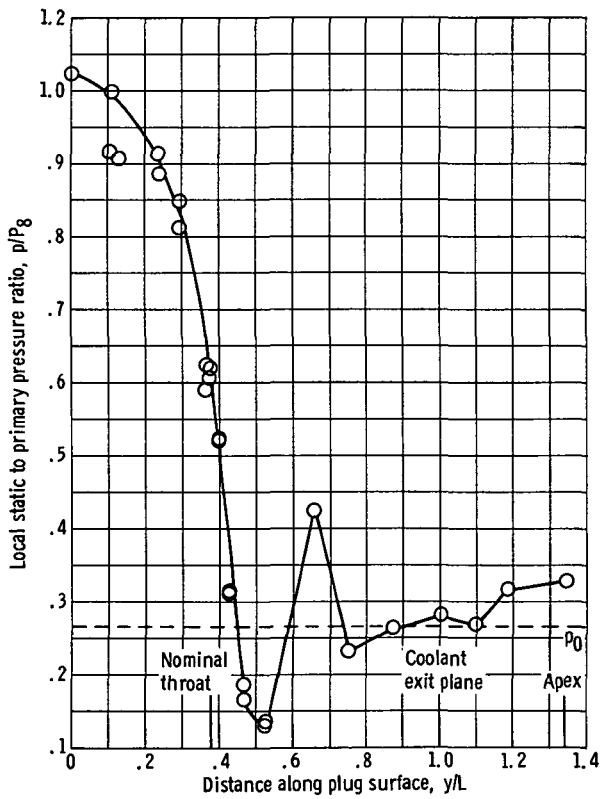

(a-3) Mach 0.89.

(a) Reheat B^+; retracted shroud ($x/\ell = -0.163$).

Figure 31. - Pressure distribution along plug surface.

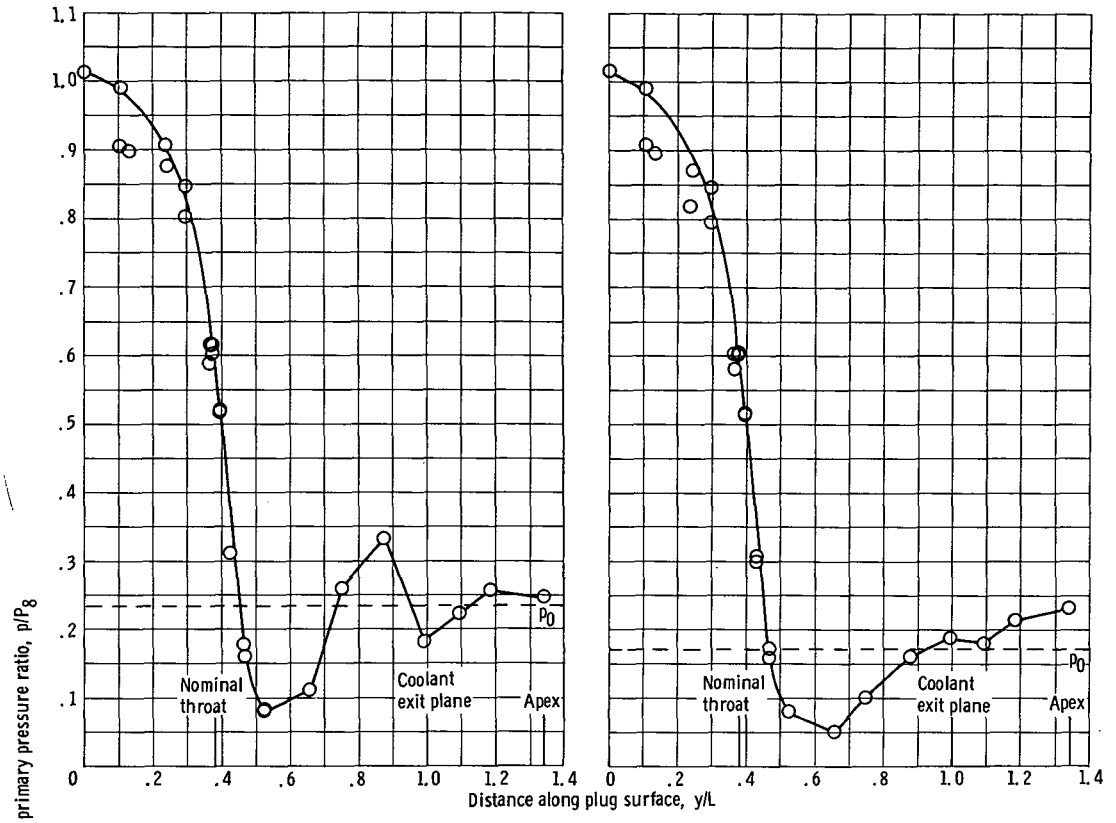

(a-4) Mach 1.01.

(a-5) Mach 1.30.

(a) Concluded.

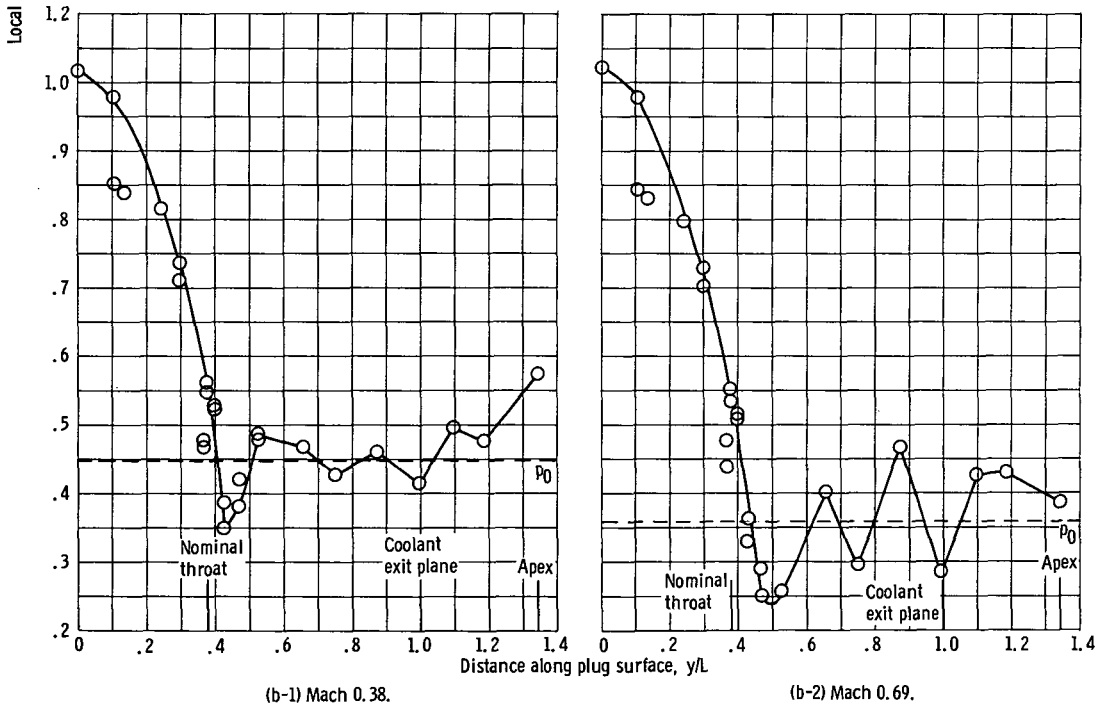

(b-1) Mach 0.38.

(b-2) Mach 0.69.

(b) Maximum afterburning; retracted shroud (x/L = -0.163).

Figure 31. - Continued.

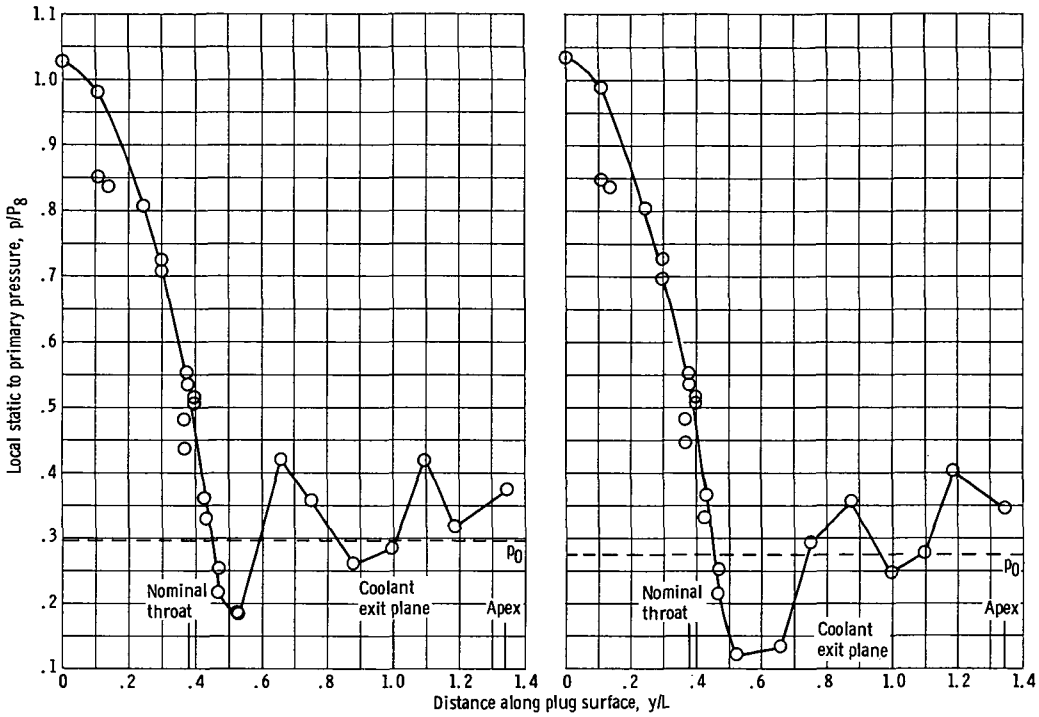

(b-3) Mach 0.90.

(b-4) Mach 0.98.

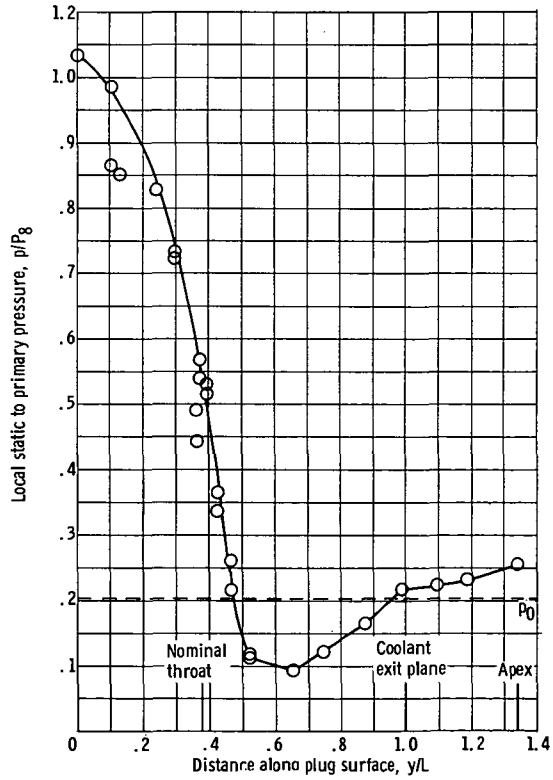

(b-5) Mach 1.29.

(b) Concluded.

Figure 31. - Continued.

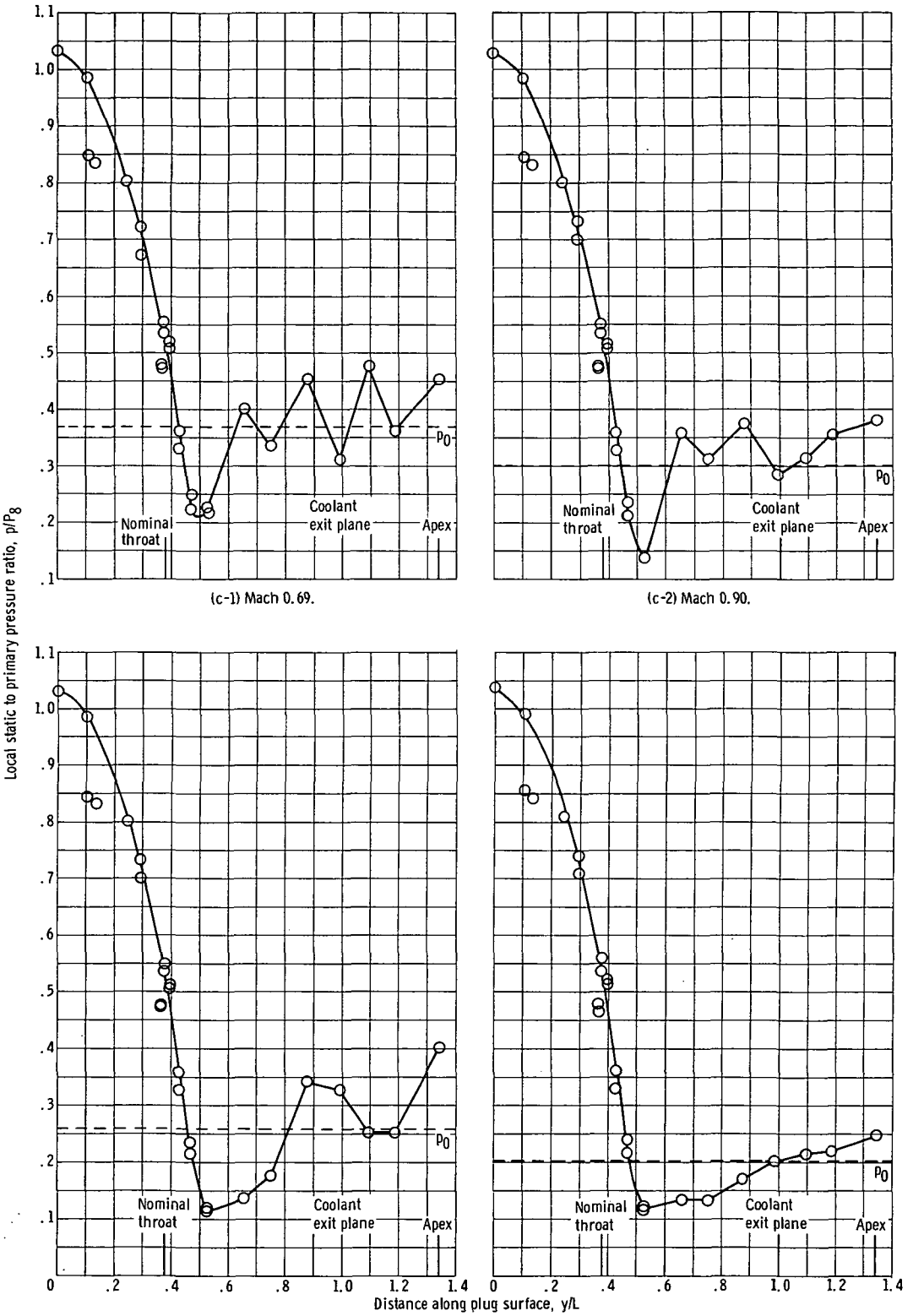

(c-1) Mach 0.69.

(c-2) Mach 0.90.

(c-3) Mach 1.04.

(c-4) Mach 1.30.

(c) Maximum afterburning; intermediate shroud (x/L = 0.163).

Figure 31. - Continued.

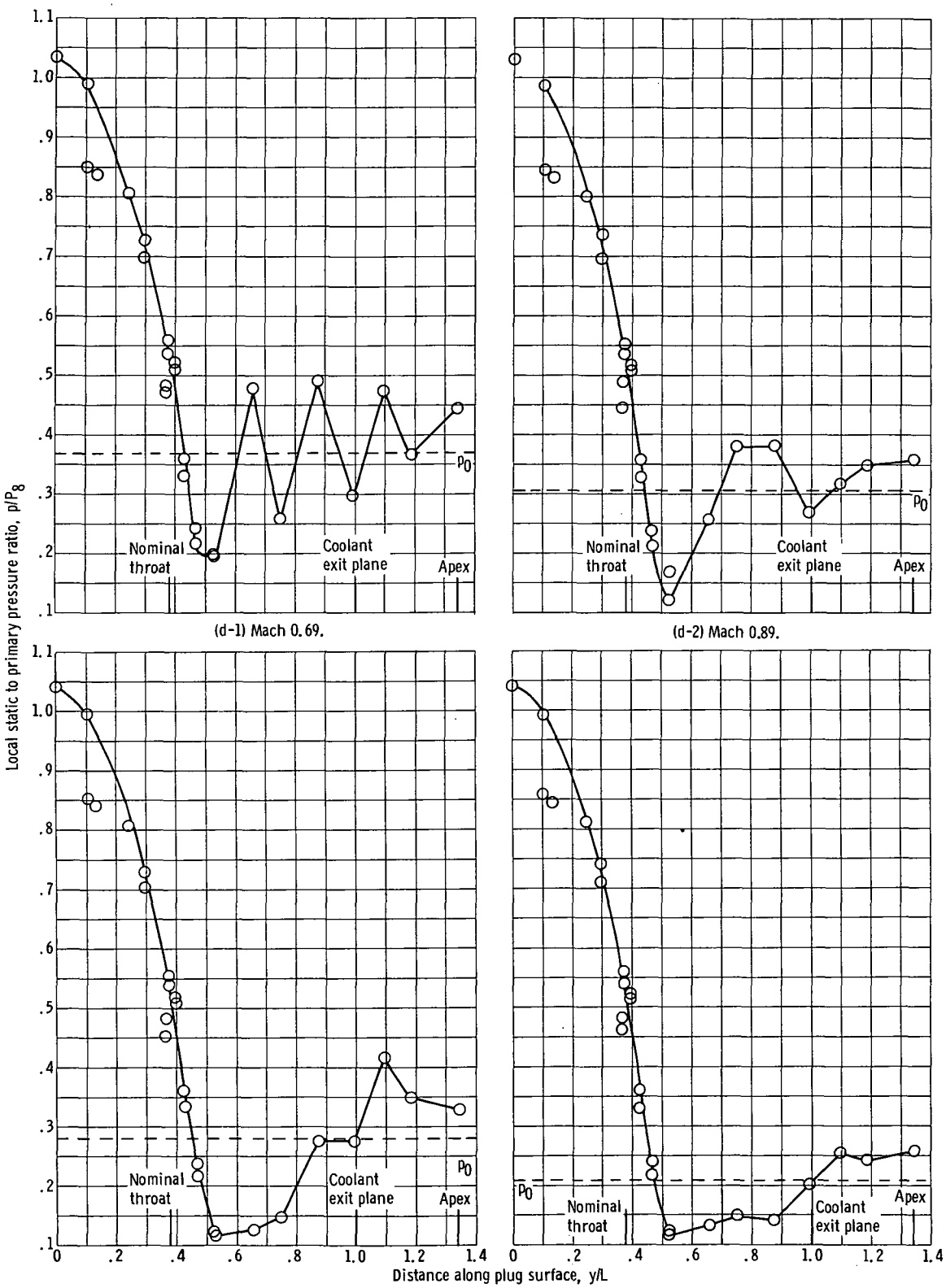

(d-1) Mach 0.69.

(d-2) Mach 0.89.

(d-3) Mach 0.98.

(d-4) Mach 1.29.

(d) Maximum afterburning; extended shroud (x/L = 0.343).

Figure 31. - Continued.

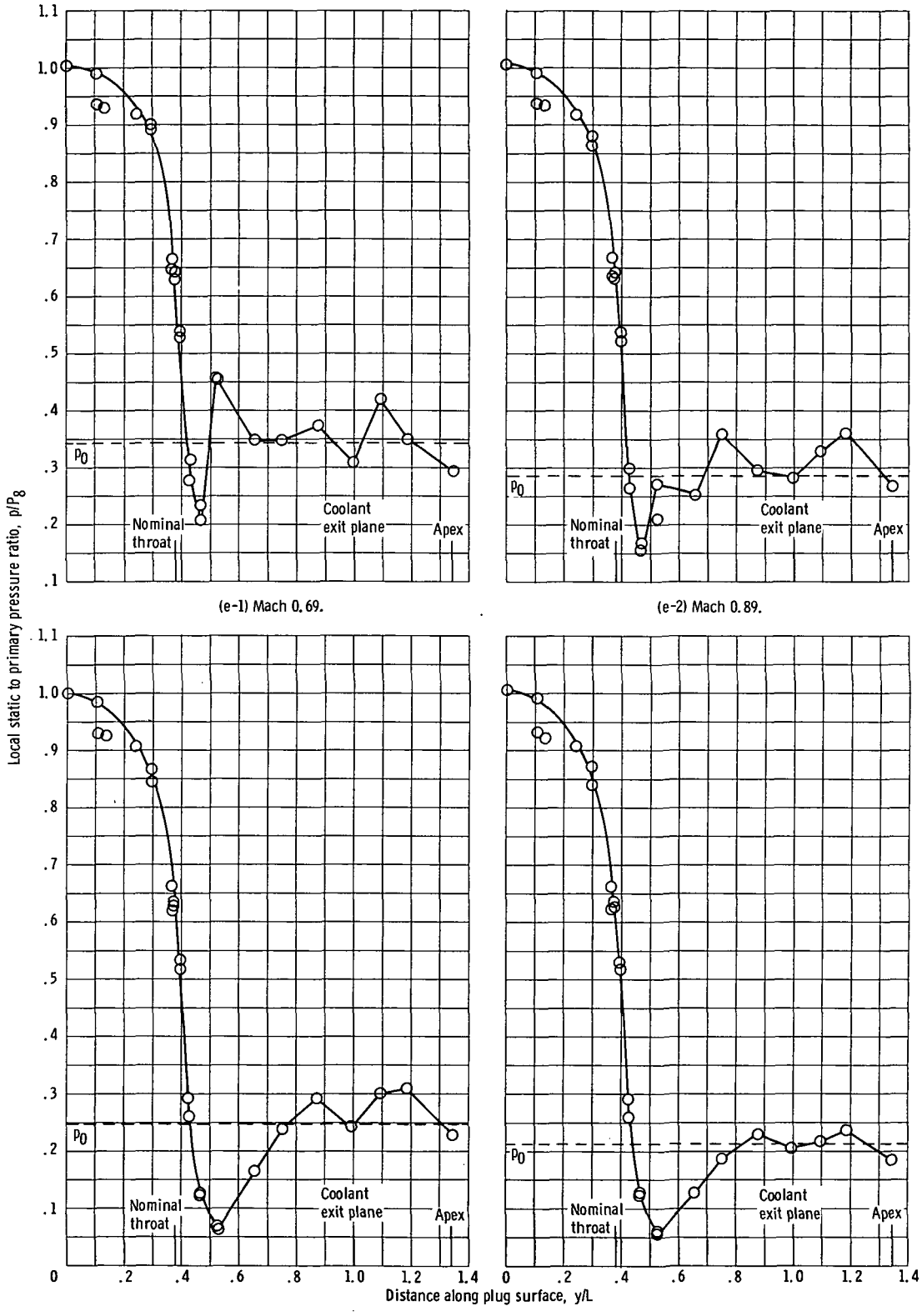

(e-1) Mach 0.69.

(e-2) Mach 0.89.

(e-3) Mach 1.02.

(e-4) Mach 1.19.

(e) Military power; retracted shroud (x/L = -0.163).

Figure 31. - Concluded.

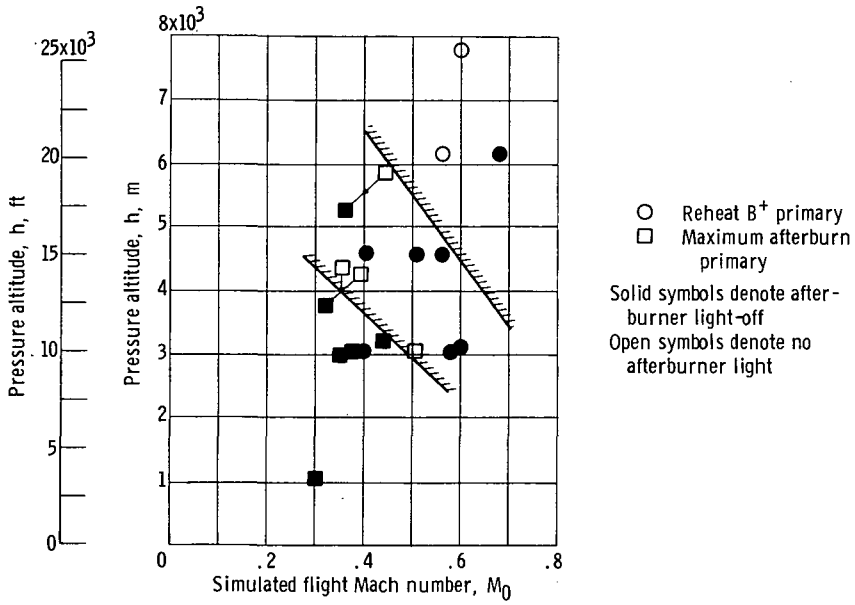

Figure 32. - J85 afterburner ignition limits with fixed exit areas obtained in altitude cell. Percent of rated engine rotor speed, 80; compressor inlet temperature, 294 K (530° R).

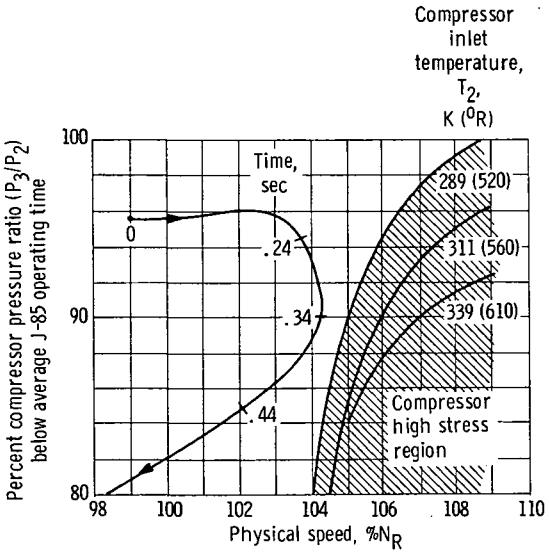

Figure 33. - J-85 transient with simulated maximum afterburning flame-out. Engine speed, 99 percent of rated turbine discharge temperature, 984 K (1770° R) before flame-out. Mechanical governor flat at 99.8 %N_R; overspeed trip at 100.5 %N_R.

NATIONAL AERONAUTICS AND SPACE ADMISTRATION
WASHINGTON, D.C. 20546

OFFICIAL BUSINESS
PENALTY FOR PRIVATE USE $300

FIRST CLASS MAIL

POSTAGE AND FEES PAID
NATIONAL AERONAUTICS AND
SPACE ADMINISTRATION

U.S.MAIL

POSTMASTER: If Undeliverable (Section 158 Postal Manual) Do Not Return

"The aeronautical and space activities of the United States shall be conducted so as to contribute . . . to the expansion of human knowledge of phenomena in the atmosphere and space. The Administration shall provide for the widest practicable and appropriate dissemination of information concerning its activities and the results thereof."

—NATIONAL AERONAUTICS AND SPACE ACT OF 1958

NASA SCIENTIFIC AND TECHNICAL PUBLICATIONS

TECHNICAL REPORTS: Scientific and technical information considered important, complete, and a lasting contribution to existing knowledge.

TECHNICAL NOTES: Information less broad in scope but nevertheless of importance as a contribution to existing knowledge.

TECHNICAL MEMORANDUMS: Information receiving limited distribution because of preliminary data, security classification, or other reasons.

CONTRACTOR REPORTS: Scientific and technical information generated under a NASA contract or grant and considered an important contribution to existing knowledge.

TECHNICAL TRANSLATIONS: Information published in a foreign language considered to merit NASA distribution in English.

SPECIAL PUBLICATIONS: Information derived from or of value to NASA activities. Publications include conference proceedings, monographs, data compilations, handbooks, sourcebooks, and special bibliographies.

TECHNOLOGY UTILIZATION PUBLICATIONS: Information on technology used by NASA that may be of particular interest in commercial and other non-aerospace applications. Publications include Tech Briefs, Technology Utilization Reports and Technology Surveys.

Details on the availability of these publications may be obtained from:

SCIENTIFIC AND TECHNICAL INFORMATION OFFICE

NATIONAL AERONAUTICS AND SPACE ADMINISTRATION

Washington, D.C. 20546